Available online at www.sciencedirect.com
ScienceDirect
International Journal of Plasticity 23 (2007) 841–875
INTERNATIONAL JOURNAL OF Plasticity
www.elsevier.com/locate/ijplas

Forming of AA5182-O and AA5754-O at elevated temperatures using coupled thermo-mechanical finite element models

Nader Abedrabbo [a], Farhang Pourboghrat [b,*], John Carsley [c]

[a] *Department of Mechanical Engineering, University of Waterloo, Ont., Canada N2L 3G1*
[b] *Department of Mechanical Engineering, Michigan State University, East Lansing, MI 48824-1226, United States*
[c] *General Motors Research and Development Center, Warren, MI 48090, United States*

Received 15 April 2005; received in final revised form 30 September 2006
Available online 28 November 2006

Abstract

A temperature-dependent anisotropic material model was developed for two aluminum alloys AA5182-O and AA5754-O and their anisotropy parameters were established. A coupled thermo-mechanical finite element analysis of the forming process was then performed for the temperature range 25–260 °C (77–500 °F) at different strain rates. In the developed model, the anisotropy coefficients for Barlat's YLD2000-2d anisotropic yield function [Barlat, F., Brem, J.C., Yoon, J.W., Chung, K., Dick, R.E., Lege, D.J., Pourboghrat, F., Choi, S.H., Chu, E., 2003. Plane stress yield function for aluminum alloy sheets – Part 1: Theory. Int. J. Plasticity 19, 1297–1319] in the plane-stress condition and the parameters for the isotropic strain hardening were established as a function of temperature. The temperature-dependent anisotropic yield function was then implemented into the commercial FEM code LS-DYNA as a user material subroutine (UMAT) using the cutting-plane algorithm for the integration of a general class of elastoplastic constitutive models [Abedrabbo, N., Pourboghrat, F., Carsley, J., 2006b. Forming of aluminum alloys at elevated temperatures – Part 2: Numerical modeling and experimental verification. Int. J. Plasticity 22 (2), 342–737]. The temperature-dependent material model was used to simulate the coupled thermo-mechanical finite element analysis of the stamping of an aluminum sheet using a hemispherical punch under the pure stretch boundary condition (no material draw-in was allowed). Simulation results were compared with experimental data at several elevated temperatures to evaluate the accuracy of the UMAT's ability to predict both forming behavior and failure locations. Two failure criteria were used in the analysis;

* Corresponding author. Tel.: +1 517 432 0189; fax: +1 517 353 1750.
E-mail address: pourbogh@egr.msu.edu (F. Pourboghrat).

0749-6419/$ - see front matter
doi:10.1016/j.ijplas.2006.10.005

the M–K strain based forming limit diagrams (ε-FLD), and the stress based forming limit diagrams (σ-FLD). Both models were developed using Barlat's YLD2000-2d anisotropic model for the two materials at several elevated temperatures. Also, as a design tool, the Genetic Algorithm optimization program HEEDS was linked with the developed thermo-mechanical models and used to numerically predict the "optimum" set of temperatures that would generate the maximum formability for the two materials in the pure stretch experiments. It was found that a higher temperature is not needed to form the part, but rather the punch should be maintained at the lowest temperature possible for maximum formability.

Keywords: Thermo-mechanical; Temperature; Material anisotropy; Plastic anisotropy; Yield function

1. Introduction

In previous papers by the authors (Abedrabbo et al., 2006a,b) a coupled thermo-mechanical model for the aluminum alloy 3003-H111 was developed using Barlat's YLD96 anisotropic model (Barlat et al., 1997) and then implemented into the finite element program LS-DYNA as a user material subroutine (UMAT). The model was shown to accurately predict forming behavior for pure stretch conditions when compared to experimental results. Comprehensive details on this work are available in Abedrabbo (2005). Motivation for the current (and previous) work stemmed from the need to use accurate numerical models in the simulation of warm forming processes to predict enhanced formability of aluminum alloys for the automotive industry.

Mass reduction has long been identified as a key priority for improving automotive fuel economy (Greene and DiCicco, 2000). However, replacing steel in the structure and body with lighter materials such as aluminum, magnesium, etc. can be costly and is not simple or straightforward. Aluminum sheet, in particular, has much lower formability at room temperature than typical sheet steel (Ayres, 1979a). High temperature forming methods based on superplastic behavior of Al–Mg alloys have been used to produce automotive closure panels that far exceed the conventional stamping formability of steel (Schroth, 2004). Superplastic formability however, requires fine-grained microstructures and slower strain rates which can affect production cost. The formability of typical 'off-the-shelf' automotive aluminum sheet alloys (5182-O and 5754-O) can be greatly improved by warm forming (Li and Ghosh, 2003) without the increased costs of refining the material microstructure. The elevated temperature produces decreased flow stress and increased ductility in the sheet, which can allow deeper drawing and more stretching to form panels without design modifications to the stamped steel product. Furthermore, the serrated flow behavior of Al–Mg sheet alloys (dynamic strain aging/PLC effect) (Robinson and Shaw, 1994) and corresponding Lüder's line surface defects that result from the interactions of solutes with mobile dislocations can be avoided by deforming the sheet metal above a critical temperature.

Numerical analysis is a critical tool for understanding the complex deformation mechanics that occur during sheet forming processes. Finite element analysis (FEA) and simulations are used in automotive design and formability processes to predict deformation behavior accurately during stamping operations. Confidence in the numerical analysis of formability depends on the accuracy of the constitutive model describing the behavior

of the material (Chung and Shah, 1992). This is especially important when the material exhibits anisotropic characteristics, as do most cold rolled sheet metals. Previous research (Zampaloni et al., 2003; Abedrabbo et al., 2005) demonstrated the importance of using appropriate material models with respect to wrinkling and ironing during the sheet hydroforming process for an Al–Mg–Si alloy (AA6111-T4). Voyiadjis and Abed (2006) proposed a coupled temperature and strain rate dependant material model for the dynamic deformations of bcc materials using von Mises yield function.

Commercially available FEA codes do not offer highly specialized material models developed for a specific material and process, and few can handle complex forming simulations that incorporate temperature-dependent materials. The simulated forming process becomes increasingly complicated when materials exhibit anisotropic behavior. The material models included in commercial FEA codes are not appropriate for simulating the thermo-mechanical forming processes of anisotropic materials such as aluminum sheet alloys. The accuracy of these material models is further compromised by the material dependence on the anisotropy coefficients that require thorough characterization under multiple loading conditions (Chung et al., 1996). This difficulty is further exacerbated when temperature effects are introduced. Because material hardening behavior and material response to loading conditions change with temperature, the anisotropy coefficients must be determined as a function of temperature to perform accurate thermo-mechanical numerical analysis for these materials.

Prior research on the elevated temperature behavior of materials in warm forming process simulation focused only on the evolution of the flow (hardening) stress (Li and Ghosh, 2003, 2004; Ayres, 1979a; Ayres and Wenner, 1979b; Painter and Pearce, 1980; Takata et al., 2000; Naka et al., 2001 and Boogaard et al., 2001). The evolution of the yield surface of aluminum alloys as a function of temperature and its effect on the anisotropy coefficients have not been fully explored. In most cases, either Hill's 1948 model (Hill, 1948) or the von Mises isotropic yield functions were used. Boogaard et al. (2001) characterized the flow stress behavior of AA5754-O with the modified power law model and also with the Bergström model. The yield surface in this case, however, was assumed to remain constant with respect to changing temperatures. Only the coefficients of the power law model were curve-fit exponentially as a function of temperature. The predictions of the material model used in the analysis underestimated the values of the punch load in both models (Power-Law and Bergström models). Čanađija and Brnić (2004) developed temperature-dependent material parameters and presented an associative coupled thermoplasticity model for the $J2$ plasticity model to represent internal heat generated due to plastic deformation. Wu et al. (2005) studied the evolution of material anisotropy of AA6111 sheet metal and the effect of pre-straining at room temperature.

Generally, heat generation due to dissipated mechanical work during plastic deformation leads to a temperature rise in the specimen (Wriggers et al., 1992; Armero and Simo, 1993). This temperature rise is a local phenomenon, however, that depends on forming speed. Abedrabbo et al. (2006a) evaluated the anisotropy coefficients during the material characterization process at the same temperature and the same forming speed, such that any thermal strain effects were included in the material model. In the current thermoforming analysis, the forming dies were maintained at a constant elevated temperature and the tests were performed at slow speeds such that the magnitude of thermal strains were of the same order as elastic strains and were negligible compared to plastic strains (see Fig. 12). Therefore, to save on computational time during thermoforming simulation, the effect of

thermal strain in the integration of the elastoplastic constitutive model was neglected. This is particularly important when performing thermoforming analysis of large industrial components.

Multiple material models can be used for representing the anisotropic behavior of aluminum alloys, e.g. Vegter and Boogaard (2006) proposed a plane stress anisotropic yield function for sheet metal by using the method of interpolation of biaxial stress states. Barlat et al. (2005) proposed a new material model (Yld2004-18p) that describes the anisotropic behavior of metals and alloys for a full stress state (3D). This new model was used by Yoon et al. (2006) to simulate the cup drawing of a circular blank sheet and accurately predicted cup height profiles (earing profiles) with six ears as compared to experimental results. In this study, the plane stress anisotropic material model proposed by Barlat et al. (2003) for describing the behavior of aluminum alloy sheets was used.

In the current research, material characterization of the anisotropy coefficients of Barlat's YLD2000-2d (Barlat et al., 2003), and the modified power-law flow stress were evaluated as a function of temperature for two 'off-the-shelf' automotive aluminum sheet alloys (5182-O and 5754-O). The temperature dependent anisotropic material model was implemented as a user material subroutine (UMAT) into the explicit part of the finite element code LS-DYNA, which was then used in a coupled thermo-mechanical finite element analysis of stamping of aluminum sheet with a hemispherical punch under pure stretch boundary conditions (with no material draw-in allowed). Deformation behavior and failure locations were compared with experimental results. An optimization program was used as a design tool to search for the optimum set of temperatures to maximize formability.

2. Anisotropic yield function

Accuracy of numerical analysis depends on the use of a constitutive model that precisely describes the behavior of the material. The importance of using an appropriate material model that captures the anisotropic behavior was demonstrated with Barlat's YLD96 model for AA6111-T4 (Abedrabbo et al., 2005).

Although YLD96 (Barlat et al., 1997) is considered to be one of the most accurate anisotropic yield functions for aluminum alloys (Lademo, 1999a; Lademo et al., 1999b) because it takes seven parameters into account in the plane-stress condition, there are some challenges with respect to FE simulations, e.g. lack of proof of convexity, and the derivatives are difficult to obtain analytically. Therefore, Barlat et al. (2003) developed a better incompressible anisotropic plasticity formulation that can guarantee convexity, simplify FE implementation and application, and take σ_0, σ_{45}, σ_{90}, r_0, r_{45}, r_{90} and σ_b into account for plane-stress conditions, where σ_0, σ_{45}, σ_{90}, and σ_b are stresses in the rolling, 45°, transverse and the balanced biaxial directions, and r_0, r_{45}, r_{90} are the plastic anisotropy parameters in the rolling, 45°, and transverse directions, respectively.

The anisotropic yield function for plane stress plasticity ($\sigma_z = \sigma_{yz} = \sigma_{zx} = 0$) can be expressed in the general form from Barlat et al. (2003)

$$\Phi = \phi' + \phi'' = 2\bar{\sigma}^a \tag{1}$$

where

$$\phi' = |X'_1 - X'_2|^a \tag{2}$$

and

$$\phi'' = |2X''_2 + X''_1|^a + |2X''_1 + X''_2|^a \tag{3}$$

with $a = 6$ and $a = 8$ for BCC and FCC materials, respectively. $\bar{\sigma}$ is the flow stress. $X'_{1,2}$ and $X''_{1,2}$ are the principal values of the linear transformations on the stress deviator X' and X'' which are defined as

$$\begin{bmatrix} X'_{xx} \\ X'_{yy} \\ X'_{xy} \end{bmatrix} = \begin{bmatrix} C'_{11} & C'_{12} & 0 \\ C'_{12} & C'_{22} & 0 \\ 0 & 0 & C'_{66} \end{bmatrix} \begin{bmatrix} S_{xx} \\ S_{yy} \\ S_{xy} \end{bmatrix} \tag{4}$$

and

$$\begin{bmatrix} X''_{xx} \\ X''_{yy} \\ X''_{xy} \end{bmatrix} = \begin{bmatrix} C''_{11} & C''_{12} & 0 \\ C''_{12} & C''_{22} & 0 \\ 0 & 0 & C''_{66} \end{bmatrix} \begin{bmatrix} S_{xx} \\ S_{yy} \\ S_{xy} \end{bmatrix} \tag{5}$$

In the previous equations, $\mathbf{C}'$ and $\mathbf{C}''$ are linear transformation matrices. S_{xx}, S_{yy} *and* S_{xy} are the components of the deviatoric stress tensor S_{ij}. The subscripts x and y represent the rolling and transverse directions of the sheet, respectively. The transformation can also apply on the stress tensor σ as

$$\begin{aligned} \mathbf{X}' &= \mathbf{C}' \cdot \mathbf{s} = \mathbf{C}' \cdot \mathbf{T} \cdot \sigma = \mathbf{L}' \cdot \sigma \\ \mathbf{X}'' &= \mathbf{C}'' \cdot \mathbf{s} = \mathbf{C}'' \cdot \mathbf{T} \cdot \sigma = \mathbf{L}'' \cdot \sigma \end{aligned} \tag{6}$$

where the transformation matrix, $\mathbf{T}$, is

$$\mathbf{T} = \begin{bmatrix} 2/3 & -1/3 & 0 \\ -1/3 & 2/3 & 0 \\ 0 & 0 & 1 \end{bmatrix} \tag{7}$$

The tensors $\mathbf{L}'$ and $\mathbf{L}''$ representing linear transformations of the stress tensor are

$$\begin{bmatrix} L'_{11} \\ L'_{12} \\ L'_{21} \\ L'_{22} \\ L'_{66} \end{bmatrix} = \begin{bmatrix} 2/3 & 0 & 0 \\ -1/3 & 0 & 0 \\ 0 & -1/3 & 0 \\ 0 & 2/3 & 0 \\ 0 & 0 & 1 \end{bmatrix} \begin{bmatrix} \alpha_1 \\ \alpha_2 \\ \alpha_7 \end{bmatrix} \tag{8}$$

and

$$\begin{bmatrix} L''_{11} \\ L''_{12} \\ L''_{21} \\ L''_{22} \\ L''_{66} \end{bmatrix} = \frac{1}{9} \begin{bmatrix} -2 & 2 & 8 & -2 & 0 \\ 1 & -4 & -4 & 4 & 0 \\ 4 & -4 & -4 & 1 & 0 \\ -2 & 8 & 2 & -2 & 0 \\ 0 & 0 & 0 & 0 & 9 \end{bmatrix} \begin{bmatrix} \alpha_3 \\ \alpha_4 \\ \alpha_5 \\ \alpha_6 \\ \alpha_8 \end{bmatrix} \tag{9}$$

The independent coefficients α_k (for k: 1–8) are all that is needed to describe the anisotropy of the material; where they reduce to 1 in the isotropic case.

Only seven coefficients are needed to account for the seven input data mentioned above, namely σ_0, σ_{45}, σ_{90}, σ_b, r_0, r_{45}, and r_{90}. The eighth coefficient can be determined by assuming

$\mathbf{C}''_{12} = \mathbf{C}''_{21}$ or $\mathbf{L}''_{12} = \mathbf{L}''_{21}$, or by using additional input data such as the ratio $r_b = \dot{\varepsilon}_{yy}/\dot{\varepsilon}_{xx}$, which characterizes the slope of the yield surface in balanced biaxial tension ($\sigma_{yy} = \sigma_{xx}$). This parameter, denoted r_b, is analogous to the r-value obtained in uniaxial tension, and can be determined with three different methods: experimental measurement, calculation from another yield function i.e. Yld96, or computation from a polycrystal model if the crystallographic texture of the material is known. The yield function coefficients are calculated with a Newton–Raphson non-linear solver, the details of which can be found in the paper by Barlat et al. (2003).

For the material model to account for changes in temperature, the anisotropy coefficients α_k which describe the state of anisotropy must be represented as a function of temperature, i.e.

$$\Phi = \bar{\sigma}(\underset{\sim}{\sigma}, T) \tag{10}$$

3. Flow stress

Flow stress ($\bar{\sigma}$) represents the size of the yield function during deformation. Metals undergoing plastic deformation at high temperatures and different strain rates should be modeled according to the physical behavior of the material (Gronostajski, 2000). An appropriate constitutive equation describing changes in the flow stress of the material depends on deformation conditions such as temperature and strain rate. Wagoner et al. (1988) proposed a flow rule that includes the strain-rate sensitivity

$$\bar{\sigma}(\bar{\varepsilon}^{\mathrm{p}}, \dot{\varepsilon}) = K(\bar{\varepsilon}^{\mathrm{p}} + \varepsilon_0)^n \left(\frac{\dot{\varepsilon}}{\varepsilon_{\mathrm{sr0}}}\right)^m \tag{11}$$

where K (strength coefficient), n (strain-hardening exponent) and m (strain-rate sensitivity index) are material constants. $\bar{\varepsilon}^{\mathrm{p}}$ is the effective plastic strain and $\dot{\varepsilon}$ is the strain rate. ε_0 is a constant representing the elastic strain to yield and $\varepsilon_{\mathrm{sr0}}$ is a constant which is a strain rate normalization factor whose value depends on the time units used in the FEA simulation (e.g. 0.001 for milliseconds). As explained in Abedrabbo et al. (2006a), the experimental value of ε_0 is very small and its values could be calculated from the values of "K" and "n".

This model was primarily selected over other types of hardening laws (e.g. Voce hardening law) because it represented the hardening behavior of the current material accurately, and it incorporated strain rate effects. Gronostajski (2000) describes different types of hardening laws that could be used (e.g. Backofen, Grosman) to represent other materials, including those with hardening saturation behavior. Recently, Hashiguchi (2005) proposed a generalized plastic flow rule that could be used as well. Håkansson et al. (2005) compared isotropic and kinematic hardening models in thermoplasticity.

To include temperature effects in the flow rule, the material constants K, n and m are expressed as a function of temperature, and the flow stress equation becomes

$$\bar{\sigma}(\bar{\varepsilon}^{\mathrm{p}}, \dot{\varepsilon}, T) = K(T)(\bar{\varepsilon}^{\mathrm{p}} + \varepsilon_0)^{n(T)} \left(\frac{\dot{\varepsilon}}{\varepsilon_{\mathrm{sr0}}}\right)^{m(T)} \tag{12}$$

The hardening model described by Eq. (12) was used assuming isotropic hardening behavior.

4. Material characterization

4.1. Materials

Chemical compositions of the two aluminum alloys (AA5182-O and AA5754-O) used in this study are shown in Table 1. All samples of each material were taken from a single lot of material. Table 2 shows the initial mechanical properties of the two aluminum alloys.

4.2. Experimental procedure

Uniaxial tests with standard ASTM-E8 rectangular dog-bone shaped samples were performed on an Instron Model 1127 screw-driven frame with a 4.5 kN load cell, 25 mm axial extensometer (50% maximum strain) and 12.7 mm transverse extensometer (30% maximum strain). The tensile samples were prepared from the aluminum sheet metal at 0° (rolling direction, RD), 45° and 90° (transverse direction, TD) from the rolling direction of the sheet. For the measurement of plastic anisotropy parameters, ASTM-E517 specifies that the test be performed at a 0.0083 s^{-1} (0.5/min) straining rate. Sample temperature was controlled with an Instron Model 3119 oven with a convection heating system. Tests were performed for several elevated temperatures in the range of 25–260 °C (77–500 °F), with the results of three tests averaged for each temperature. It should be mentioned that only small variations in the stress–strain behavior were noticed between the three tests for each temperature. These tensile tests were performed at a fixed ambient temperature. Generally heat generation due to dissipation of plastic work, related to high strain rate testing, will affect the temperature of the specimen. However, since the strain rate at which the tests are performed is low, this effect can be ignored and a uniform specimen temperature assumed. To study the strain-rate sensitivity of the material, uniaxial tests under several strain rates (0.001–0.08 s^{-1}) were performed at each temperature. Bulge testing was performed on sheet samples from the same lot of material in order to determine σ_b at room temperature. Experimental calculation of the balanced biaxial data at elevated temperature is under development. Bulge stress σ_b at elevated temperatures was estimated using the anisotropic yield function YLD91 model (Barlat et al., 1991). Barlat's YLD91 model requires only the plastic anisotropy parameters (R_0, R_{45} and R_{90}) as input to the model. By using these

Table 1
Chemical composition of aluminum alloys (wt%)

	Al	Mg	Mn	Fe	Si	Cu	Ni	Ti	Zn
AA5182-O	Bal	4.3	0.34	0.21	0.03	<0.01	<0.01	<0.01	<0.01
AA5754-O	Bal	3.0	0.24	0.26	0.03	0.02	<0.01	<0.01	<0.01

Table 2
As-received mechanical properties of AA5182-O and AA5754-O

Material	Thickness (mm)	UTS (MPa)	Yield strength (MPa)	Total elongation (%)
AA5182-O	1.15	266	119	22
AA5754-O	1.00	234	102	21

values and setting $\sigma_{xx} = \sigma_{yy}$ (balanced biaxial condition) and $\sigma_{xy} = 0$ in the model, the values of σ_b that satisfies this condition can be solved for using numerical solution methods. With a value of the exponent in YLD91 of $a = 8$ (FCC material), the numerical solution would involve solving for the roots of an 8th-order polynomial. However, only two of the eight solutions would be real and useful. These two roots are equal in value but opposite in sign. More details about the experimental procedure and on using tensile data in extracting material properties can be found in Abedrabbo et al. (2006a).

4.3. Flow rule (hardening model) results

Figs. 1 and 2 show the true stress–strain behavior at several temperatures for the rolling direction for both materials. As can be seen from the figures, the two materials exhibit serrated flow curves at lower temperatures. This is due to dynamic strain aging, which leads to stretch marks in a product after the forming process. Dynamic strain ageing can be explained as the interaction between dislocations and solute atoms. The dislocation movement is hampered by the solute magnesium atoms, leading to a higher initial yield stress (Boogaard et al., 2001). If dislocations move slowly (at low strain rates), the solute atoms can migrate to the dislocations while they are arrested at other obstacles or solutes. This further hampers the dislocation movement. As temperature increases, flow stress of the material decreases with a corresponding increase in the elongation to failure. This is due to the increase in the mobility of the solutes which eliminates the serrated flow behavior. Correspondingly no stretch marks develop at elevated temperatures. The softening in the two materials starts to occur at temperatures over 93 °C for the 5182-O material, and over 121 °C for the 5754-O material.

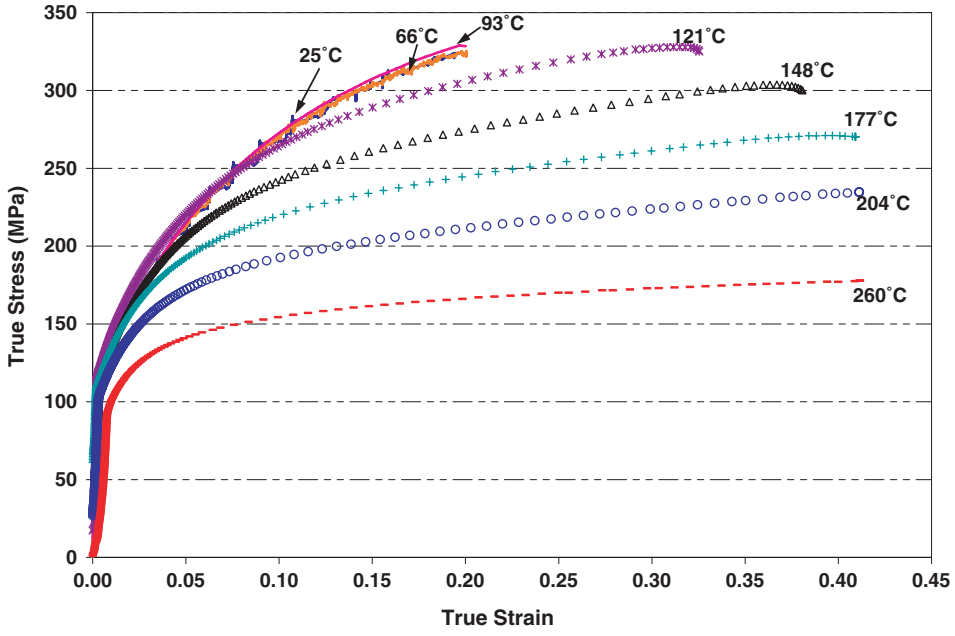

Fig. 1. True stress–strain curves of AA5182-O at several elevated temperatures for the rolling direction.

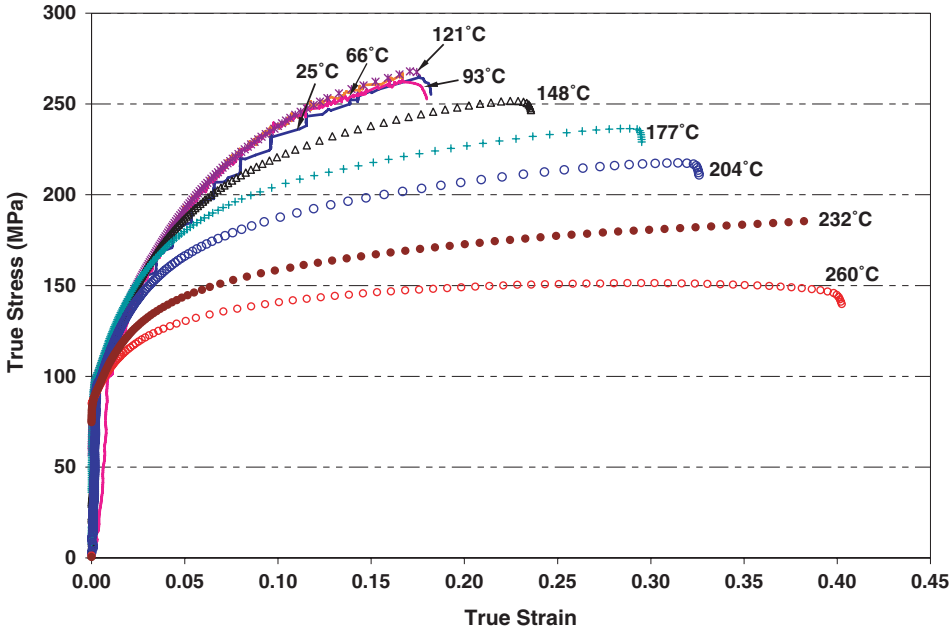

Fig. 2. True stress–strain curves of AA5754-O at several elevated temperatures for the rolling direction.

Strain-rate sensitivity was measured at different temperatures using two methods: tests were performed at different strain-rates (from 0.001 to 0.08 s^{-1}) with multiple samples, and the "Jump-Rate Test" method (Wagoner and Chenot, 1996) where the crosshead speed was increased to produce a "jump" in the strain rate at some predetermined level of strain with a single sample. Fig. 3 shows the true stress-true strain curves for the AA5182-O material at 260 °C (500 °F) in the rolling direction at different strain rates using the first method, while Fig. 4 shows results for the AA5182-O material using the jump-rate test method at several elevated temperatures in which crosshead speed jumps were 10–50–150 mm/mm/min. As seen in the figures, the material exhibited very small strain-rate sensitivity at room temperature, but with increasing temperature, the material became more strain rate sensitive. This was also observed for the AA5754-O material.

From the results of the uniaxial tension tests performed at different constant strain rates, and at several elevated temperatures, values for the Holloman hardening rule (K, n, ε_0 and m) and the plastic anisotropy parameters (R_θ) were calculated as a function of temperature. Figs. 5 and 6 show the experimental values of "K" and "n" for the two materials as a function of temperature. For each material, two linear curve fits were used to represent the coefficients for the complete temperature range, e.g. for AA5182-O, both K and n coefficients were fit using two linear functions; one for the temperature range of 25–93 °C, and another for 93–260 °C. This was done to account for the tensile behavior noticed in Figs. 1 and 2 where the material started to soften and serrated flow behavior diminished above a certain temperature.

Fig. 7 shows the variation of the strain-rate sensitivity index, m, as a function of temperature for both materials. At lower temperatures, m values were very small, indicating the material is strain-rate insensitive; but at higher temperatures, the material exhibited

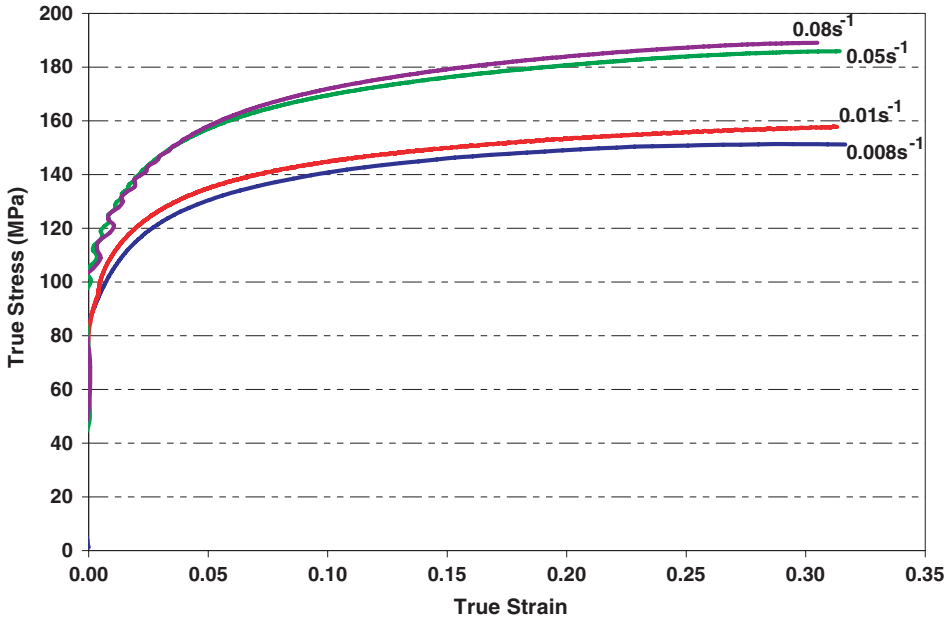

Fig. 3. True stress-true strain data of AA5182-O from uniaxial tests at 260 °C (500 °F) at several strain rates for the rolling direction.

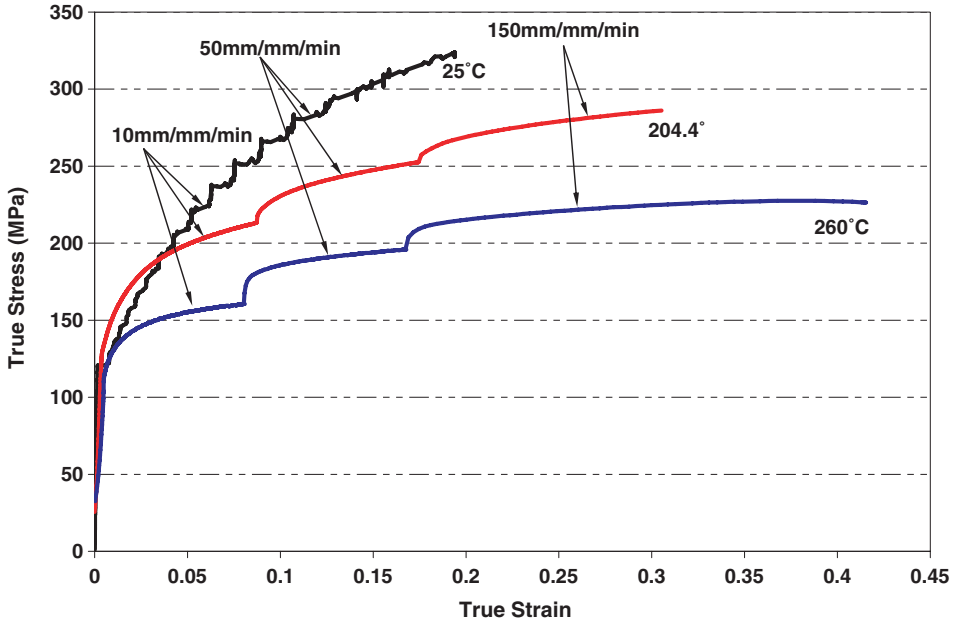

Fig. 4. True stress-true strain data for AA5182-O from uniaxial tests using the jump-rate strain method. The jumps in crosshead speed were 10–50–150 mm/mm/min.

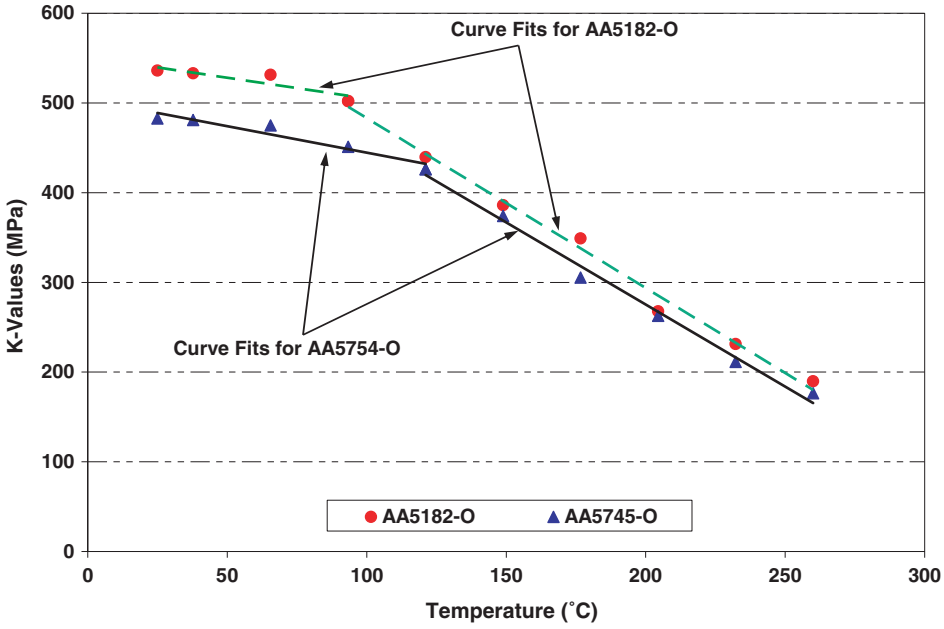

Fig. 5. Strength coefficient (K) for AA5182-O and AA5754-O along the rolling direction as a function of temperature at 0.5/min strain rate.

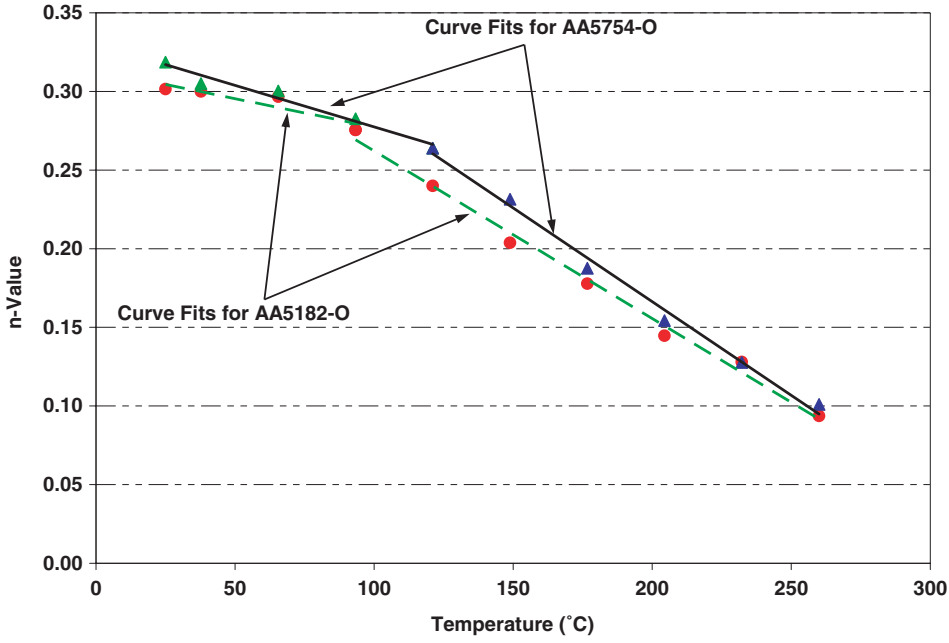

Fig. 6. Strain-hardening exponent (n) for AA5182-O and AA5754-O along the rolling direction as a function of temperature at 0.5/min strain rate.

a significant sensitivity to strain-rate. Exponential functions, as shown on the graph, were used to represent the behavior of m as a function of temperature for each material. For the finite element simulation, values of K, n and m from the rolling direction only were used to represent isotropic hardening.

Tables 3 and 4 show a summary of the equations used to fit the hardening parameters for the flow rule shown in Eq. (12), along the rolling direction, as a function of temperature for both materials. Curve fitting at 45° and the transverse directions were not required, since only the values of hardening in the rolling direction were used in the finite element simulation.

Figs. 8 and 9 show the variation of the plastic anisotropy parameters R_0, R_{45} and R_{90}, measured at a straining rate of 0.0083 s^{-1} (0.5/min), for both materials with respect to temperature. Values of plastic anisotropy parameters R_θ higher than 1.0 indicate good formability and resistance to thinning. As can be seen from Figs. 8 and 9, the values of R_0, R_{45} and R_{90} increase with temperature, which suggests that the formability of the aluminum sheet is also enhanced at elevated temperature.

4.4. Barlat's yield 2000-2d anisotropy coefficients

Because temperature has a significant effect on material properties (Abedrabbo et al., 2006a,b), it is imperative to apply a temperature-dependent constitutive model for accurate analysis of warm forming. It is also necessary that this temperature-dependent constitutive model be used in a coupled thermo-mechanical finite element analysis of warm forming processes where the thermal analysis provides temperature as input to the mechanical

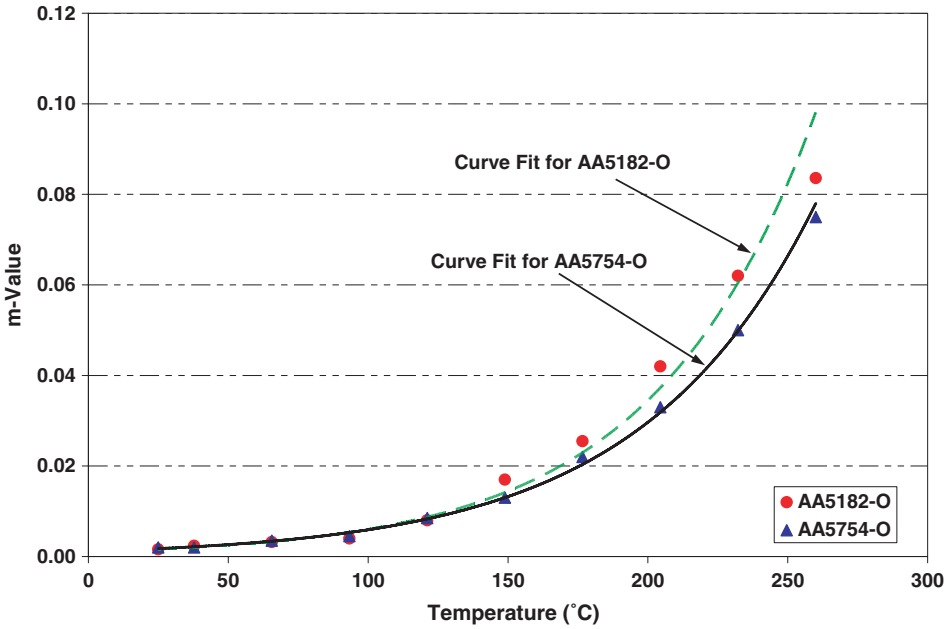

Fig. 7. Strain-rate sensitivity index (m) for AA5182-O and AA5754-O along the rolling direction as a function of temperature. Exponential curve fits used.

Table 3
AA5182-O: summary of equations used to fit hardening parameters for the power law flow rule

Hardening parameter	Rolling direction, 0°	Temperature range (°C)	Unit
$K_1(T)$	$551.2 - 0.4623 * T$	25–93	MPa
$K_2(T)$	$672.3 - 1.8926 * T$	93–260	
$n_1(T)$	$0.3135 - 0.000363 * T$	25–93	
$n_2(T)$	$0.3687 - 0.001065 * T$	93–260	
$m(T)$	$0.00106 * \exp(0.01743 * T)$	25–260	

Temperatures in °C.

Table 4
AA5754-O: summary of equations used to fit hardening parameters for the power law flow rule

Hardening parameter	Rolling direction, 0°	Temperature range (°C)	Unit
$K_1(T)$	$503.7 - 0.592 * T$	25–93	MPa
$K_2(T)$	$641.3 - 1.829 * T$	93–260	
$n_1(T)$	$0.3304 - 0.000529 * T$	25–93	
$n_2(T)$	$0.4048 - 0.001192 * T$	93–260	
$m(T)$	$0.00118 * \exp(0.0161 * T)$	25–260	

Temperatures in °C.

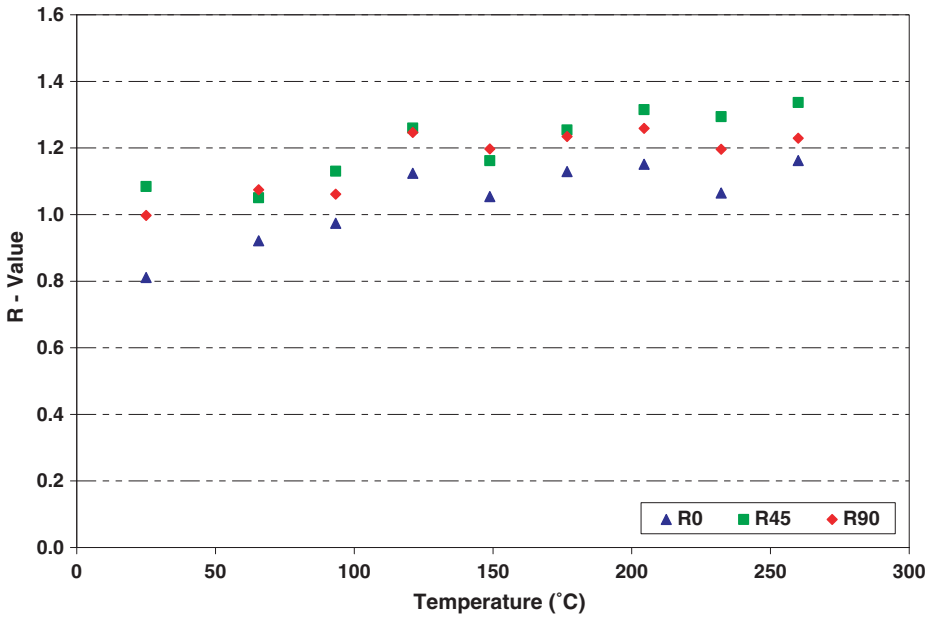

Fig. 8. Plastic anisotropy parameters (R_θ) for AA5182-O as a function of temperature, calculated at 0.5/min strain rate (ASTM-E517).

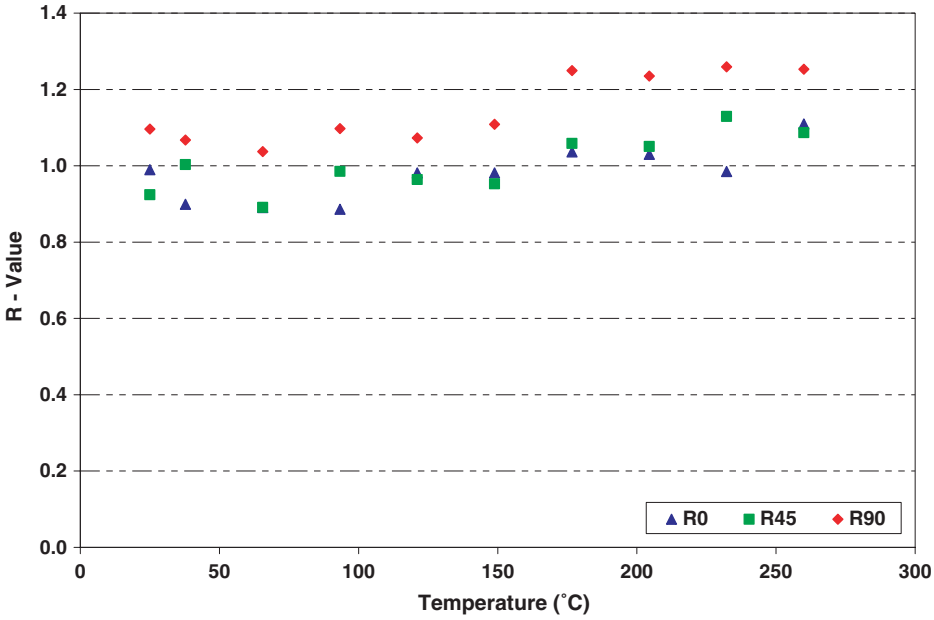

Fig. 9. Plastic anisotropy parameters (R_θ) for AA5754-O as a function of temperature, calculated at 0.5/min strain rate (ASTM-E517).

model (Čanađija and Brnić, 2004). It is from such a coupled analysis that deformation stresses corresponding to both thermal and mechanical deformation could be accurately calculated. In order to develop an anisotropic material model for use in a coupled thermo-mechanical finite element analysis of sheet metal forming processes, the anisotropy coefficients of a yield function must be represented as a function of temperature.

Tensile test data were used to calculate the anisotropic coefficients for Barlat's YLD2000-2d model at several temperatures. In order for the constitutive model to accurately represent the aluminum sheet at large strains, the anisotropic coefficients describing the behavior of the material, i.e. α_k (k: 1–8), must be calculated using the results from the tensile tests at several elevated temperatures. Four stress-states, uniaxial tension along the rolling, 45°, and transverse directions and balanced biaxial stress (Green et al., 2004) provide the required data points (Barlat et al., 2003).

The yield stress could be used as input data instead of the flow stress. However, it may be difficult to accurately measure yield stress in the bulge test as well as in uniaxial tension because the slope of the stress–strain curve is steep and yielding is not always a discrete event in many aluminum alloys (Barlat et al., 1997). Also, the yield stress is associated with very small plastic strain and might not reflect the anisotropy of the material over a larger strain range. For these reasons, flow stresses at equal amounts of plastic work ($W_b = W_u$) were selected as input data rather than yield stress (Abedrabbo et al., 2006a). In this work, values of $W_b = W_u = 30$ MPa per unit volume for both materials were used to extract flow stresses σ_0, σ_{45} and σ_{90}. The normalized values σ_0/σ_0, σ_{45}/σ_0, σ_{90}/σ_0 and σ_b/σ_0 were then used as input to calculate the anisotropy coefficients of the yield function. Flow stresses extracted at different values of W would not significantly change those stress ratios, and

therefore consistent results can be obtained as long as sufficiently large values of W are used. Fig. 10 shows the stress values σ_0, σ_{45}, σ_{90} and σ_b for AA5754-O. Details for calculating the anisotropy coefficients for Barlat YLD2000-2d can be found in Barlat et al. (2003).

Curve-fitting was used to fit the anisotropy coefficients calculated at discrete temperatures for both materials. Fig. 11 shows a sample plot for one of the YLD2000-2d coefficients (α_1 for AA5754-O) as a function of temperature. The fitting functions used for all anisotropy coefficients α_k (k: 1–8) are shown in Table 5 for AA5182-O and Table 6 for AA5754-O.

From a first glance at Fig. 11, it seems that the anisotropy coefficient of Barlat YLD2000-2d is fluctuating randomly without any apparent trend. This is attributed to the fact that the experimental data needed to calculate the anisotropic coefficients do not linearly increase with temperature. Fig. 10 shows that stress values decrease with temperature, while plastic anisotropy parameters (R_0, R_{45} and R_{90}) in Figs. 8 and 9 increase with temperature. These opposing trends cause anisotropy coefficients of the yield function to fluctuate. Therefore, higher order fitting functions are necessary to capture these variations.

To summarize, the yield function represented by Eq. (1) can be written as

$$\Phi(\bar{\sigma}, \bar{\varepsilon}^{\mathrm{p}}, \dot{\varepsilon}, T) = \bar{\sigma}(\underset{\sim}{\sigma}, T) - H(\bar{\varepsilon}^{\mathrm{p}}, \dot{\varepsilon}, T) = 0 \tag{13}$$

where H is the hardening rule defined by Eq. (12). T is the temperature calculated during the thermal analysis step and supplied as input to the UMAT during the structural analysis segment of the simulation.

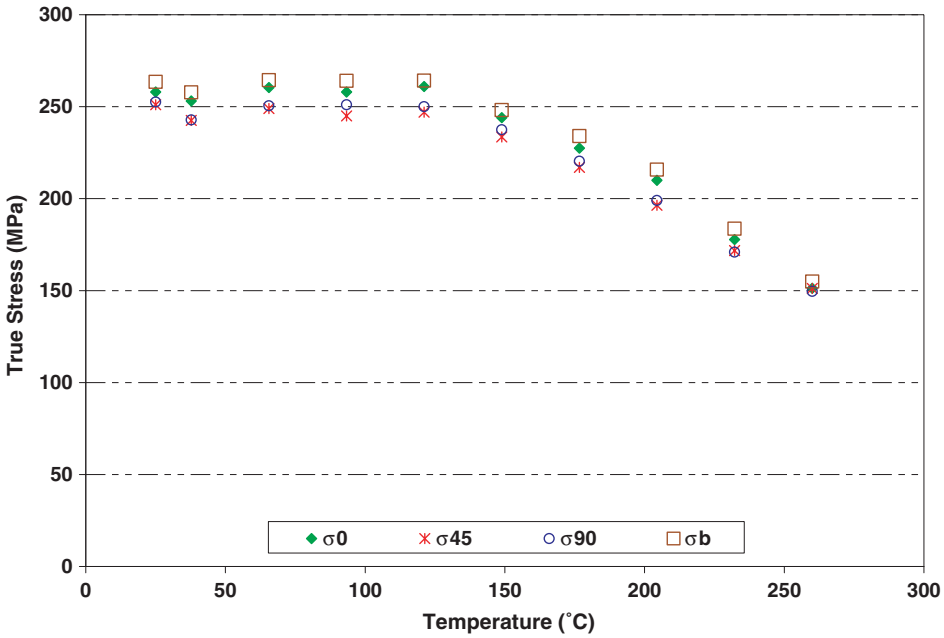

Fig. 10. Stress values at equal values of plastic work (30 MPa/unit-vol.) as a function of temperature for AA5754-O.

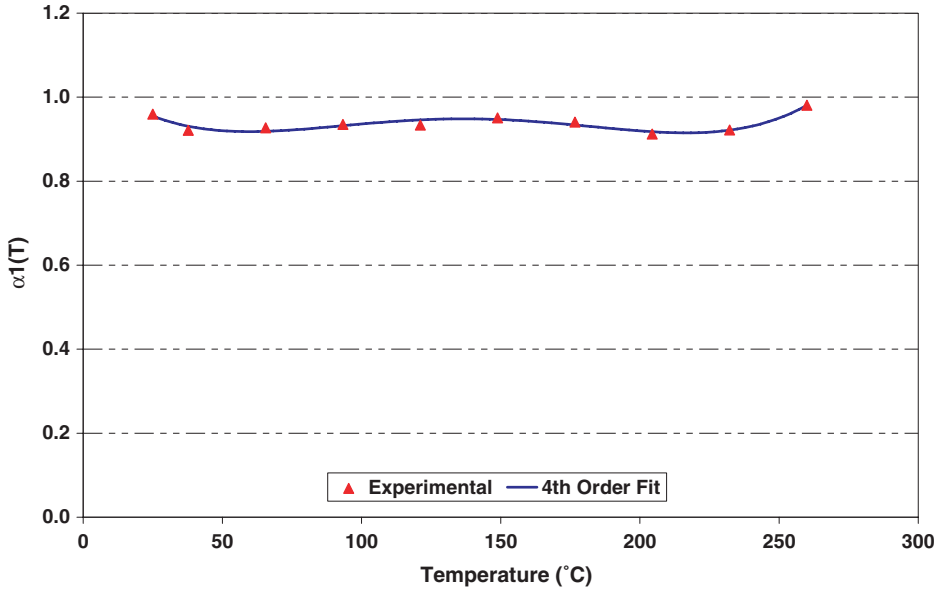

Fig. 11. Plot of (α_1) as a function of temperature for AA5754-O. A 4th-order polynomial curve fit is shown also.

Table 5
Barlat YLD2000-2d material model anisotropy coefficients for AA5182-O as a function of temperature

Anisotropy coefficient	4th-Order fit
α_1	$0.955 - 6.777\text{E}-04T + 1.466\text{E}-05T^2 - 8.537\text{E}-08T^3 + 1.675\text{E}-10T^4$
α_2	$1.004 + 1.807\text{E}-03T - 2.046\text{E}-05T^2 + 9.573\text{E}-08T^3 - 1.773\text{E}-10T^4$
α_3	$0.839 + 2.072\text{E}-03T - 1.533\text{E}-05T^2 + 4.131\text{E}-08T^3 - 1.509\text{E}-11T^4$
α_4	$0.963 + 1.127\text{E}-03T - 1.298\text{E}-05T^2 + 5.546\text{E}-08T^3 - 8.314\text{E}-11T^4$
α_5	$0.988 + 7.583\text{E}-04T - 1.130\text{E}-05T^2 + 5.756\text{E}-08T^3 - 9.806\text{E}-11T^4$
α_6	$0.887 + 3.018\text{E}-03T - 3.205\text{E}-05T^2 + 1.377\text{E}-07T^3 - 2.075\text{E}-10T^4$
α_7	$1.040 - 7.955\text{E}-04T + 1.383\text{E}-05T^2 - 7.786\text{E}-08T^3 + 1.402\text{E}-10T^4$
α_8	$1.166 - 3.596\text{E}-03T + 5.096\text{E}-05T^2 - 2.797\text{E}-07T^3 + 4.985\text{E}-10T^4$

Temperatures in °C.

Table 6
Barlat YLD2000-2d material model anisotropy coefficients for AA5754-O as a function of temperature

Anisotropy coefficient	4th-Order fit
α_1	$1.058 - 5.979\text{E}-03T + 8.573\text{E}-05T^2 - 4.655\text{E}-07T^3 + 8.456\text{E}-10T^4$
α_2	$0.952 + 6.757\text{E}-03T - 9.986\text{E}-05T^2 + 5.633\text{E}-07T^3 - 1.054\text{E}-09T^4$
α_3	$1.027 - 6.585\text{E}-03T + 9.949\text{E}-05T^2 - 5.626\text{E}-07T^3 + 1.046\text{E}-09T^4$
α_4	$0.986 + 5.234\text{E}-04T - 5.749\text{E}-06T^2 + 2.303\text{E}-08T^3 - 3.433\text{E}-11T^4$
α_5	$0.978 + 1.203\text{E}-03T - 1.569\text{E}-05T^2 + 7.766\text{E}-08T^3 - 1.317\text{E}-10T^4$
α_6	$0.969 + 2.623\text{E}-04T + 5.397\text{E}-08T^2 - 1.384\text{E}-08T^3 + 3.902\text{E}-11T^4$
α_7	$0.977 + 2.229\text{E}-03T - 3.012\text{E}-05T^2 + 1.686\text{E}-07T^3 - 3.241\text{E}-10T^3$
α_8	$0.993 + 6.042\text{E}-03T - 8.151\text{E}-05T^2 + 4.492\text{E}-07T^3 - 8.602\text{E}-10T^4$

Temperatures in °C.

5. Stress integration for elasto-plasticity using anisotropic yield function

The effect of thermal strain in the integration of the elastoplastic constitutive model was neglected due to the fact that its magnitude is very small, and that its neglect should not affect the simulation results. Fig. 12 shows the plot of thermal, elastic and plastic strain increments calculated for the case of thermoforming at the elevated temperature of 204 °C (400 °F) for AA5754. It could be seen that thermal strains are between 2 and 3 orders of magnitude smaller than plastic strains and the assumption to neglect them in the stress integration algorithm is justified.

Stress integration of the elastoplastic yield functions is explored in numerous publications (Armero and Simo, 1993; Auricchio and Taylor, 1999; and Tuğcu and Neale, 1999). Implementation of the stress integration algorithm for YLD96 was previously described in detail (Abedrabbo et al., 2006b). This algorithm, which is based on the incremental theory of plasticity (Chung and Richmond, 1993; Yoon et al., 1999; Han et al., 2003), can be applied to a general class of yield functions, and was used to implement the UMAT for the YLD2000-2d model. Yoon et al. (2004) provides details for the stress integration for the YLD2000-2d yield function.

In the general commercial FEA codes, e.g. LS-DYNA and ABAQUS, the strain increment $(\underset{\sim}{\dot{\varepsilon}}_{n+1})$, the previous stress state value $(\underset{\sim}{\sigma}_n)$ and any *history variables* saved at the previous stress update step are provided at the beginning of each time step. The new strain increment is then assumed to be elastic and an elastic predictor stress state "trial stress" is calculated through the customary elasticity relations. Using the cutting plane algorithm, the

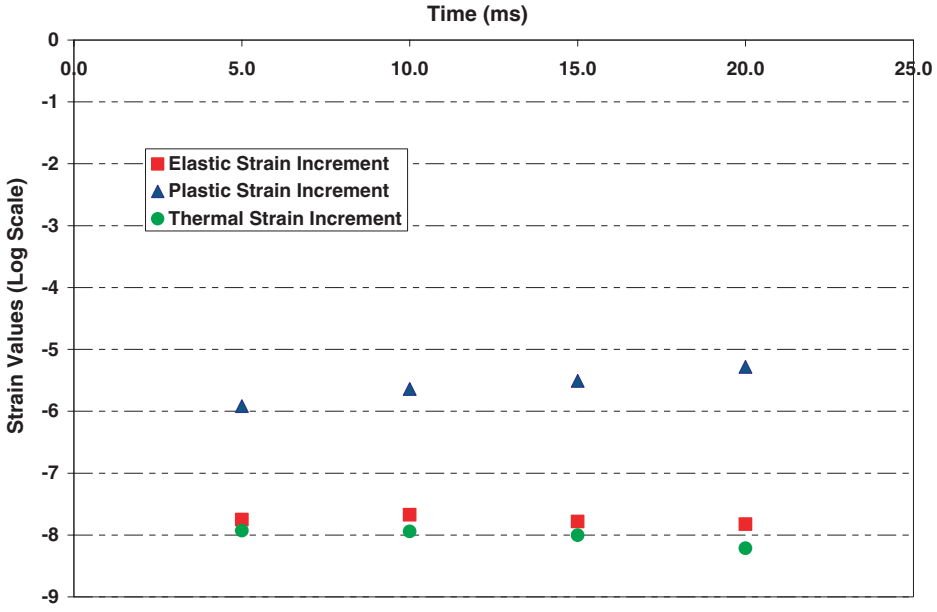

Fig. 12. Computed values of elastic, plastic and thermal strain increments for an element at different times. The results shown correspond to thermoforming analysis at the elevated temperature of 204 °C (400 °F) for AA5754-O.

actual stress state is then restored (plastic corrector) and other plastic variables are calculated.

The basic steps in the numerical procedure for iteratively integrating the elastoplastic constitutive equations for rate independent plasticity with an associated flow rule are:

$$\dot{\underset{\sim}{\varepsilon}}^{\mathrm{e}}_{n+1} = \dot{\underset{\sim}{\varepsilon}}_{n+1} \tag{14}$$

$$\dot{\underset{\sim}{\sigma}} = \underset{\approx}{C} : \dot{\underset{\sim}{\varepsilon}}^{\mathrm{e}}_{n+1} \tag{15}$$

$$\text{Associative flow rule} : \dot{\underset{\sim}{\varepsilon}}^{\mathrm{p}} = \dot{\lambda}\frac{\partial \Phi}{\partial \underset{\sim}{\sigma}} \tag{16}$$

$$\text{Yield function} : \Phi \leqslant 0 \tag{17}$$

$$\text{Normality parameter} : \dot{\lambda} \geqslant 0 \tag{18}$$

$$\text{Kuhn–Tucker condition} : \dot{\lambda}\Phi = 0 \tag{19}$$

$$\text{Consistency condition} : \dot{\lambda}\dot{\Phi} = 0 \tag{20}$$

where $\underset{\sim}{\sigma}$, $\dot{\underset{\sim}{\varepsilon}}^{\mathrm{e}}$ and $\dot{\underset{\sim}{\varepsilon}}^{\mathrm{p}}$ are the stress, elastic strain rate/increment and plastic strain rate/increment, respectively. $\underset{\approx}{C}$ is the fourth-order elastic tensor which is assumed to be constant. The associated flow rule is expressed by Eq. (16) in which $\dot{\lambda}$ is the plastic multiplier and Φ is the yield function as defined by Eq. (13). The yielding criterion and the loading–unloading conditions are expressed in the standard Kuhn–Tucker form (Simo and Hughes, 1998) in which the constraints in Eqs. (17)–(20) are satisfied.

It should be noted that planar anisotropy was incorporated into the formulation for sheet forming simulations using the plane stress version of Barlat's YLD2000-2d model. When the deformation of the workpiece is not limited to the plane of the sheet, it is important to impose the requirement that for the plane-stress application, the in-plane material axes have to remain in the plane of the sheet during the deformation (Tuğcu and Neale, 1999). In the current application using the LS-DYNA FEA code, the initial anisotropy of the material is introduced by defining two local vectors in the plane of the material. Then all transformations into the element local system are performed prior to entering into this user material subroutine. Transformations back to the global system are performed after exiting the user material subroutine (Hallquist, 1999).

Accuracy of the current YLD2000-2d model was compared to the YLD96 model (Abedrabbo et al., 2006a,b) for the warm forming of multiple materials (AA3003-H111, AA5754-O and AA5182-O), and results for both models were similar. The new model (YLD2000-2d) however, has some clear advantages over the YLD96 model. The YLD2000-2d model was easier to implement as a UMAT, provided better stability, and most importantly, improved solution time for the FEA model by almost 50%, which is a big advantage in solving large scale models.

6. Experimental procedure

Limiting dome height (LDH) tests were conducted using a modified Interlaken 30-ton double action servo press (model 75). Detailed information about the press and the forming procedure can be found elsewhere (Abedrabbo et al., 2005; Zampaloni et al., 2003). The experimental setup was used to form 101.6 mm (4 in.) diameter hemispherical cups

from 177.8 mm (7 in.) diameter round blanks of both materials under pure stretch conditions. The blank was placed over a lock bead and clamped with a blank holding force (BHF) of approximately 267 kN (60,000 lbf) to prevent the sheet from drawing in during the pure stretch experiments.

Heating elements with an active control device were used in the LDH machine in order to elevate the temperature of the dies and the blank. The active control was achieved with two thermocouples linked to the die and blank system. Additional thermocouples were installed to directly measure the temperature of both the blank and the punch during the forming process. These critical measurements were needed to perform accurate numerical analysis of the experiment.

The experimental procedure at a specific elevated temperature is as follows. The blank was clamped in place with three heating element bands wrapped around the perimeter of the dies, which were insulated to minimize heat loss to the environment. The desired temperature was set and maintained for about 20 min or until a constant and isothermal condition was achieved. Temperature was monitored using several thermocouples within the system. The temperature of the punch was not controlled independently, and for the current research, the punch temperature was found to be cooler than the blank. With an isothermal blank condition, the punch was then actuated to stretch the blank while recording the punch force–displacement curve. This process was repeated several times for each temperature to establish repeatability. Pure stretch experiments were performed at several elevated temperatures in the range of 25–204 °C (77–400 °F).

7. Coupled thermo-mechanical finite element model

Finite element analysis (FEA) was performed using the commercial finite element code LS-DYNA (Hallquist, 1999) to understand the deformation behavior of the aluminum sheet during the thermoforming process. The UMAT option was used to build the user material subroutine in FORTRAN, which was then linked with the library files supplied by LSTC. Hypermesh? was used to create the finite element mesh, assign the boundary conditions and to build the LS-DYNA input deck for the analysis. The full size finite element model used approximately 55,000 four- and three-node shell elements. The punch, die, and the blank-holder were created using rigid materials (Material 20 in LS-DYNA).

The thermal analysis was performed first, during which the temperature of each element was calculated and supplied as input to the UMAT. Using the temperature value for each element, the temperature dependent anisotropic material model coefficients were calculated. Before every structural iteration step, two thermal analysis steps were performed with a controlled time step to ensure that the temperature update was adequate.

In this research, a linear fully implicit transient thermal analysis was performed with the diagonal scaled conjugate gradient iterative solver type in LS-DYNA. The die and blank materials were assumed to behave with isotropic thermal properties. Table 7 shows the thermal properties defined in the analysis for the dies and the blank.

The lower die, upper die (blank holder) and punch were assigned a constant temperature boundary condition throughout the analysis, with the punch being set at a lower temperature than both dies based on experimental data. The blank was given an initial temperature boundary condition equal to the upper and lower dies. Table 8 shows the values of the boundary conditions of the dies and punch as well as the initial conditions for

Table 7
Thermal properties of material used in numerical analysis

Material	Density (kg/m^3)	Specific heat capacity (J/kg K)	Thermal conductivity (J/m K)
Rigid dies (FE)	7.85E3	450	70
Blank (Al)	2.71E3	904	220

Table 8
Measured temperatures of dies (lower die and blank holder), punch and blank during experiments

Test temperature (°C)	Dies temperature (°C)	Punch temperature (°C)	Blank temperature (°C)
25	25	25	25
38	38	38	38
93	94	91	93
149	147	122	140
177	172	141	174
204	205	171	202

the blank. Thermal properties were assigned to the contact surfaces to enable heat transfer at appropriate areas of contact between the blank and tooling during the analysis. Subsequently, areas of the blank that made contact with the punch lost heat to the punch while the unsupported regions of the blank remained at higher temperatures. In the numerical simulation, no heat transfer was allowed to occur with the surrounding air since in the experimental setup the heaters maintained the temperatures of the dies at a constant level.

Since the experiments and simulations were done at quasi-static speeds (low strain rate), any heat generation due to dissipation of plastic work related to blank deformation were assumed to be small and have minimal impact on the blank temperature and, therefore, was not included in the analysis.

8. Failure prediction

Two approaches were used in the current analysis to determine when failure occurs. Strain based forming limit diagrams (ε-FLD) were calculated for both materials with the Marciniak–Kuczynski (M–K) model (Marciniak and Kuczynski, 1967) using Barlat's YLD2000-2d anisotropic yield function and appropriate coefficients for each temperature. In the current analysis, an imperfection parameter of 0.996 was used in the M–K method. This imperfection parameter value was chosen based on the microstructural analysis of aluminum alloys performed by Barlat and Richmond (2003) where experimental data was found to best agree with a value of 0.996. Kim et al. (2003) also studied the formability of AA5182 and from experimental tests they found the imperfection value to be 0.997. The FLD calculated using this number accurately predicted failure observed in the experiments. Yao and Cao (2002) describe methods for extracting FLD for prediction of forming limit curves using an anisotropic yield function. In the forming process, if the loading path is sufficiently close to linear (proportional loading) then a strain-based FLD can be used to assess failure of the sheet. For a general forming process in which the loading path may not be linear (non-proportional loading), it would be necessary to either integrate the M–K model into the FEM analysis to assess each element separately according to

its loading path, or to use a stress-based FLD, which is less sensitive to strain path (Stoughton, 2001). The former case, however, is very expensive to use in FEM analysis. Therefore, the second failure criterion used in this research is the stress based forming limit diagram (σ-FLD). A review of different types of σ-FLD and their use in FEA can be found in Stoughton and Zhu (2004).

Strain based FLD curves (ε-FLD) used in this study were based on the Voce hardening law, which offers a more conservative prediction of failure compared to the power law (Abedrabbo et al., 2006b). Fig. 13 shows the ε-FLD curve at different temperatures for AA5182-O. As seen from the figure, increasing temperature effectively raises the forming limit curves, suggesting that the materials can be stretched to higher levels of strain before failure occurs. The ε-FLD at each temperature is supposed to be calculated using different strain rate boundary conditions for the M–K theory for strain-rate sensitive materials. However, due to the invariance principle, the strain distribution is not affected by different boundary conditions if the rate sensitivity index m is constant (Chung and Wagoner, 1986; Chung and Wagoner, 1998) and temperature rise due to dissipating plastic work is ignored. Therefore, one FLD is used for each temperature in this work which was obtained from the base strain rate.

Although in the current analysis, use of the strain based FLD is sufficient, the motivation for developing the stress based forming limit diagrams (σ-FLD) stems from the need to develop an accurate failure method to be used in conjunction with the developed coupled thermo-mechanical material models in the simulation of warm forming of automotive parts. In such parts where geometry is complex, the assumption of proportional loading

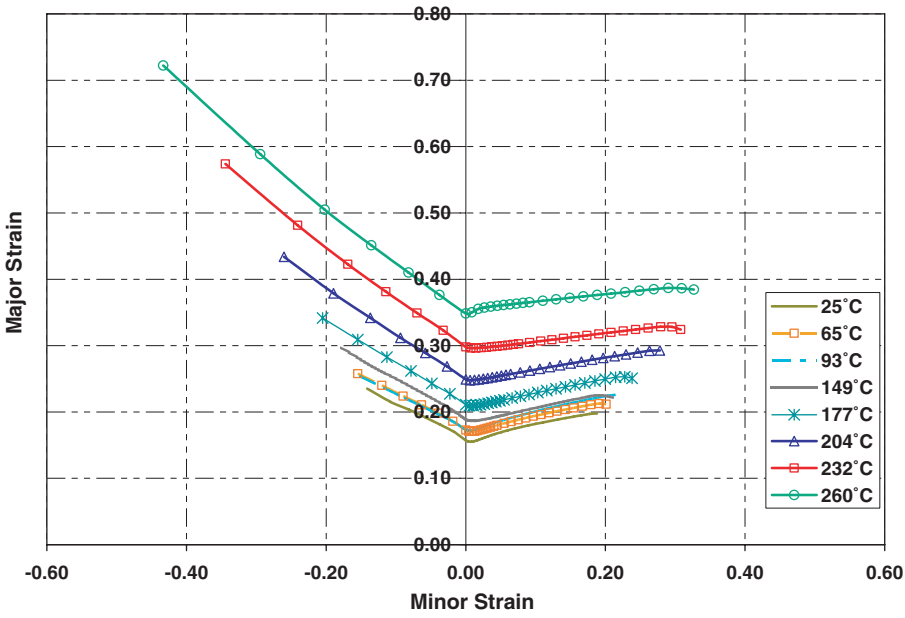

Fig. 13. Forming limit diagrams (ε-FLDs) for AA5182-O based on the M–K model, Barlat's YLD2000-2d anisotropic yield function, and Voce hardening law at several elevated temperatures.

does not always hold, and the strain based FLD cannot be used with certainty to predict failure. Therefore, a path-independent failure method should be used. Stoughton (2001) proposed a method to transform the path-dependent strain based FLD into a path-independent stress based FLD. The equations used in calculating the stress based FLD using Barlat's YLD2000-2d as used in Stoughton (2001) is as follows.

The effective stress function for YLD2000-2d is obtained from the yield function as in Eq. (1). First, Eq. (1) is written as

$$\Phi = \left(\frac{1}{2}|X'_1 - X'_2|^a + |2X''_2 + X''_1|^a + 2X''_1 + X''_2|^a\right)^{\frac{1}{a}} \tag{21}$$

where

$$\begin{aligned} X'_1 &= L'_{11}\sigma_1 + L'_{12}\sigma_2 \\ X'_2 &= L'_{21}\sigma_1 + L'_{22}\sigma_2 \end{aligned} \tag{22}$$

and

$$\begin{aligned} X''_1 &= L''_{11}\sigma_1 + L''_{12}\sigma_2 \\ X''_2 &= L''_{21}\sigma_1 + L''_{22}\sigma_2 \end{aligned} \tag{23}$$

then

$$\begin{aligned} \bar{\sigma} = 2^{\frac{-1}{a}}[&|L'_{11}\sigma_1 - L'_{21}\sigma_1 + L'_{12}\sigma_2 - L'_{22}\sigma_2|^{(a)} + |2L''_{11}\sigma_1 + L''_{21}\sigma_1 + 2L''_{12}\sigma_2 + L''_{22}\sigma_2|^{(a)} \\ &+ |L''_{11}\sigma_1 + 2L''_{21}\sigma_1 + L''_{12}\sigma_2 + 2L''_{22}\sigma_2|^{(a)}] \end{aligned} \tag{24}$$

The effective strain rate cannot be expressed as a simple function of strain tensor components, but the definition of the plastic work rate can be used as follows

$$\dot{\bar{\varepsilon}} = \frac{1}{\bar{\sigma}}(\sigma_1\dot{\varepsilon}_1 + \sigma_2\dot{\varepsilon}_2) = \frac{\dot{\varepsilon}_1}{\xi}(1 + \alpha\rho) \tag{25}$$

The ratio between the effective stress and major stress is

$$\begin{aligned} \xi(\alpha) = \frac{\bar{\sigma}}{\sigma_1} = 2^{\frac{-1}{a}}[&|L'_{11} - L'_{21} + L'_{12}\alpha - L'_{22}\alpha|^{(a)} + |2L''_{11} + L''_{21} + 2L''_{12}\alpha + L''_{22}\alpha|^{(a)} \\ &+ |L''_{11} + 2L''_{21} + L''_{12}\alpha + 2L''_{22}\alpha|^{(a)}] \end{aligned} \tag{26}$$

where

$$\alpha = \frac{\sigma_2}{\sigma_1} \tag{27}$$

and

$$\rho = \frac{\dot{\varepsilon}_2}{\dot{\varepsilon}_1} \tag{28}$$

The relationship between α and ρ cannot be expressed explicitly, therefore, numerical solution methods must be used. By using the definition of ρ and the plastic strain rates defined as

$$\dot{\varepsilon}_{ij} = \dot{\bar{\varepsilon}}\frac{\partial\bar{\sigma}}{\partial\sigma_{ij}} \tag{29}$$

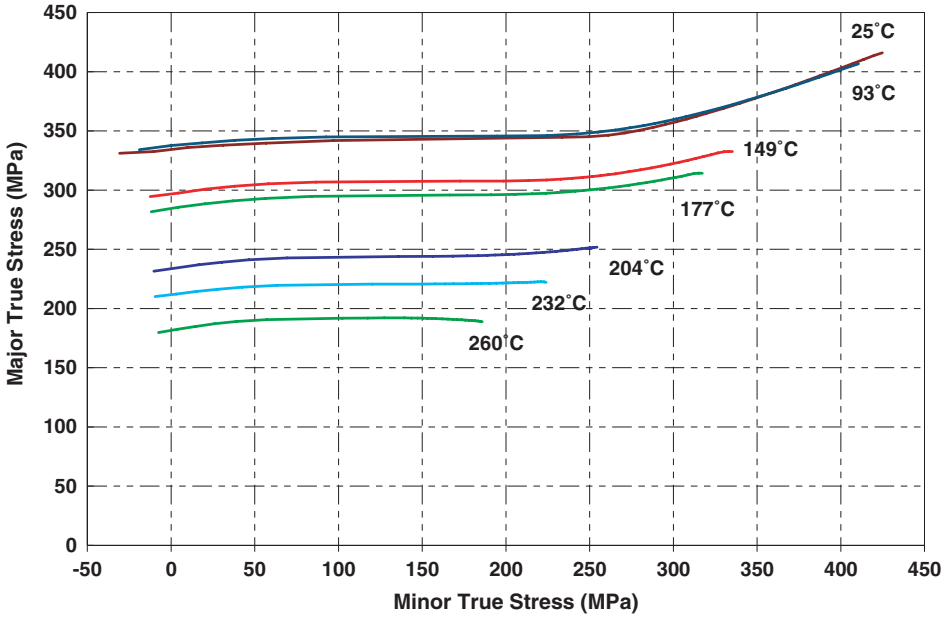

Fig. 14. Stress based forming limit diagrams (σ-FLDs) for AA5182-O using a power law model and Barlat's YLD2000-2d anisotropic yield function at several elevated temperatures.

The value of α can be calculated, for a given value of $\rho = \dot{\varepsilon}_2/\dot{\varepsilon}_1$, using Eqs. (28) and (29) combined with Eq. (27). The numerical simulation for $a = 8$ (FCC material) would involve solving for the roots of a 7th-order polynomial. However, only one of the seven solutions would be real and useful. After the value of α is found, it is substituted into Eq. (26) in order to calculate ξ. The value of σ_1 is then found from

$$\sigma_1 = \frac{\bar{\sigma}(\bar{\varepsilon}(\dot{\varepsilon}_1, \dot{\varepsilon}_2))}{\xi(\alpha(\dot{\varepsilon}_1, \dot{\varepsilon}_2))} \tag{30}$$

Knowing the values of σ_1 and α, Eq. (27) can be used to calculate the value of σ_2. This procedure was done for all temperatures and both materials. Fig. 14 shows the stress based FLDs (σ-FLDs) for the AA5182-O material at several elevated temperatures.

It should be noted that the stress based FLD values can be extracted simultaneously during the calculation of the strain based FLD using the M–K method. However, the approach explained above can be used to calculate the stress based FLD for the YLD2000 yield function as post-processing, if only strain based FLD data points were available.

9. Numerical vs. experimental results

Finite element analysis of the pure stretch experiments was performed with the thermal-structural finite element model described previously using the temperature-dependent user material subroutine (UMAT) of Barlat's YLD2000-2d anisotropic yield function. The purposes of the numerical analysis were first to check the validity of the assumption that

thermal strains are negligible in the thermoforming process, and then to verify the accuracy of both the FEA model and the developed UMAT to predict failure in the aluminum sheet at elevated temperatures. Temperatures of the dies, punch, and blank used in the numerical analysis were as listed in Table 8. This was done to insure accurate analysis corresponding to the experimental tests.

Figs. 15 and 16 show the experimental and the fully coupled thermo-mechanical simulation results of pure stretching of AA5182-O at room temperature (25 °C) with failure punch depth and failure locations indicated. The punch depth at which the sheet failed in the numerical analysis was 24 mm (0.95 in.), which compares well with the experimental result of 24 mm. Figs. 17 and 18 show the experimental and fully coupled thermo-mechanical simulation results of pure stretching of AA5182-O at a temperature of 149 °C (300 °F) with failure punch depth and failure locations indicated. Again the experimental results accurately agree with the numerical prediction of failure location and forming depth at this elevated temperature. Fig. 19 shows a comparison between experimental and numerical results of the punch load vs. punch depth curve at several elevated temperatures for AA5182-O. As could be seen from this plot, the fully coupled thermo-mechanical model was capable of accurately predicting the punch load curves. In Fig. 19, the end of the solid line (numerical analysis) indicates the predicted failure point.

Figs. 20 and 21 show the experimental results and the fully coupled thermo-mechanical simulation of pure stretch for AA5754-O at a temperature of 177 °C (350 °F), indicating the failure punch depths and failure locations, which confirm that the simulation agrees with experimental observations. As seen from these figures, the fully coupled thermo-mechanical finite element analysis model was able to predict accurately both the failure depth and location in the sheet at various temperatures for both materials.

Failure predictions, as shown in Figs. 16, 18 and 21, are based on ε-FLD. These two figures show the contours of minor and major strain distribution for each element. Red

Fig. 15. Pure stretch experimental results using the 101.6 mm (4 in.) hemispherical punch at 25 °C (77 °F) for AA5182-O. Punch depth at failure is shown.

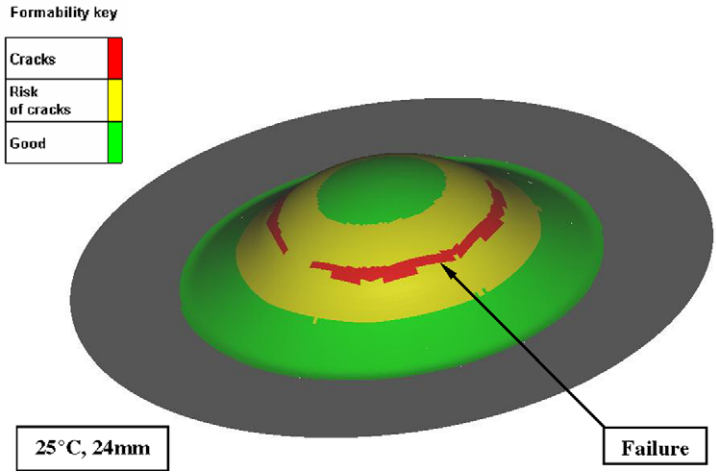

Fig. 16. Finite element result from a fully coupled thermo-mechanical simulation of thermo-forming at 25 °C (77 °F) for AA5182-O. Graph shows contour plots of formability using strain based FLD. Failure location is shown. The sheet failed where the strains crossed the ε-FLD curve at the punch depth of 24 mm.

Fig. 17. Pure stretch experimental results using the 101.6 mm (4 in.) hemispherical punch at 149 °C (300 °F) for AA5182-O. Punch depth at failure is shown.

regions indicate failure where elements crossed the forming limit curve. Failure predictions using the σ-FLD for these simulations produced the same results as the ε-FLD. It should be noted that other formability limiting causes, the actual material ductility or other failure modes (e.g. through-thickness shear) can also be included as a predictive method for failure in such analysis. However, only the physics of the instability criterion of Marciniak and Kuczynski is used in the theoretical analysis in this paper.

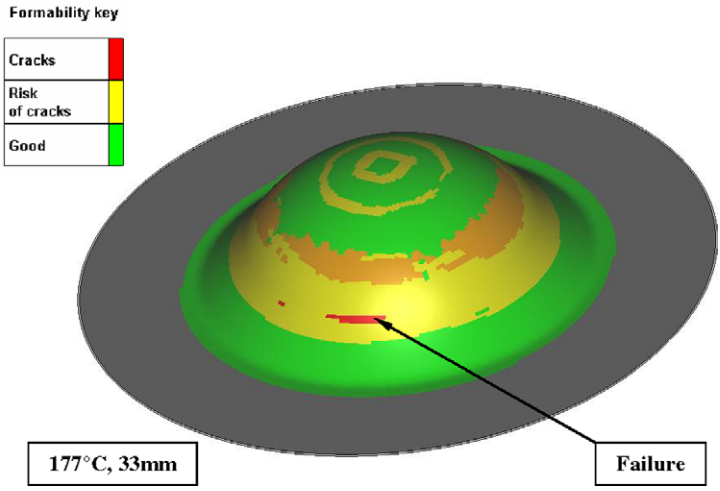

Fig. 18. Finite element result from a fully coupled thermo-mechanical simulation of thermo-forming at 149 °C (300 °F) for AA5182-O. Graph shows contour plots of formability using strain based FLD. Failure location is shown. The sheet failed where the strains crossed the ε-FLD curve at the punch depth of 33 mm (1.1 in.).

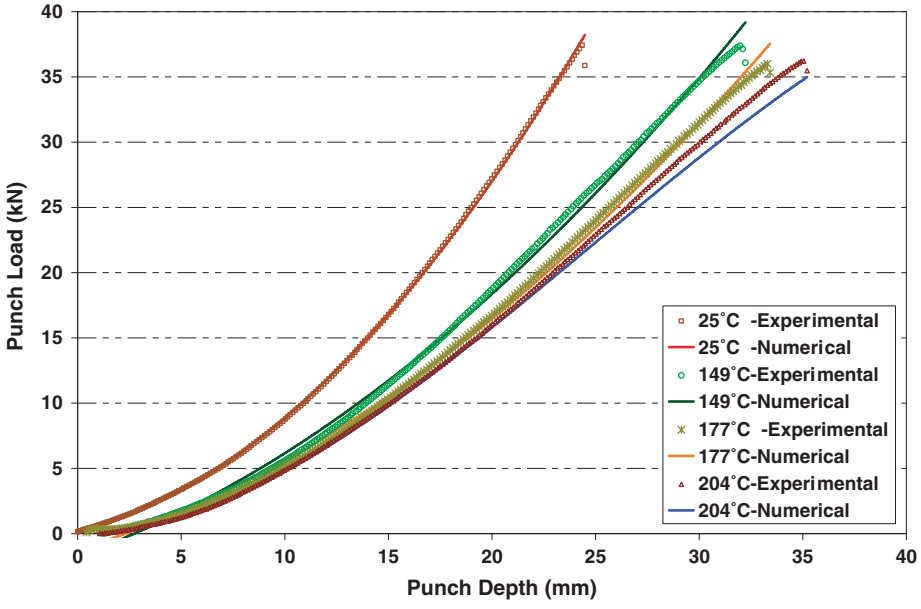

Fig. 19. Punch force vs. punch depth for the hemispherical punch stretch experiments at several elevated temperatures for AA5182-O. Numerical results closely match the experimental results. The end of the solid line (numerical analysis) indicates the predicted failure point.

Fig. 20. Pure stretch experimental results using the 101.6 mm (4 in.) hemispherical punch at 177 °C (350 °F) for AA5754-O. Punch depth at failure is shown.

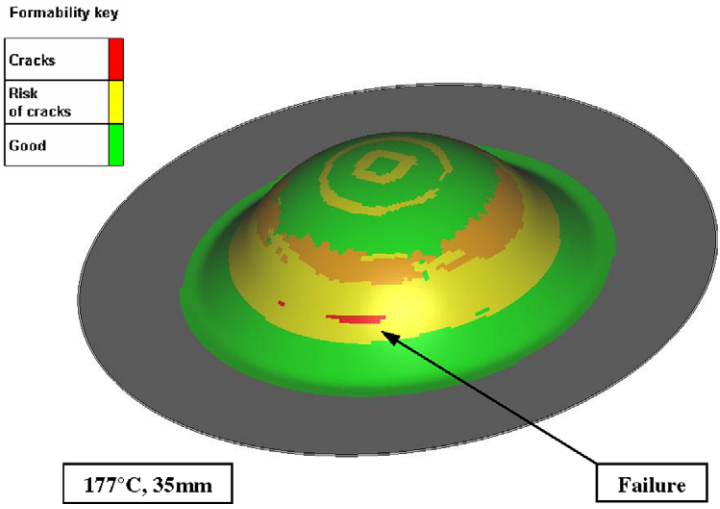

Fig. 21. Finite element result from a fully coupled thermo-mechanical simulation of thermo-forming at 177 °C (350 °F) for AA5754-O. Graph shows contour plots of formability using strain based FLD. Failure location and punch depth at failure are shown. The sheet failed where the strains crossed the ε-FLD curve at the punch depth of 35 mm (1.38 in.).

10. Process parameters optimization

In the previous section, temperatures assigned to different sections of the forming process, i.e. punch, dies, and blank, in the numerical analysis were measured directly from the experimental tests as listed in Table 8. This was done to insure accurate analysis

corresponding to the warm forming experiments, and to establish the accuracy of the developed coupled thermo-mechanical material models. The other objective for developing these constitutive material models was to apply them to formability simulation for warm forming complex automotive parts.

Many complex automotive parts that are impossible to form with aluminum alloys at room temperature could be fabricated using the warm forming process without any shape defects, i.e. fracture, wrinkling, etc. The challenge however is to determine the optimum forming temperature. To manually search for these optimum temperatures, based on intuition and experience, is very time consuming and tedious, and often does not lead to an optimal solution within a reasonable time. Therefore, an integrated approach to the problem comprised of the finite element analysis model of the warm forming process, a failure model, and an optimization code is needed. In such a numerical study, there are no guidelines in assigning temperatures for the different components; rather, the determination of these temperatures would be part of the design process. Therefore, an automatic optimization method should be utilized to predict the temperature sets that would generate a solution of the warm forming problem without any defects. Once the numerical process gives a suitable solution; the acquired temperatures can then be used to validate the process experimentally.

In this section, an approach is presented in which the warm forming process was optimized using a Genetic Algorithm (GA) search method. The goal of the study was to maximize formability of the hemispherical punch by identifying the optimal temperatures for each component while satisfying the forming limit diagram (FLD). In the current process, either the strain-based FLD (ε-FLD) or the stress-based FLD (σ-FLD) could be used because the process can be considered to have proportional loading conditions. However, in a complex part analysis, where non-proportional loadings can exist, it is preferred to use a stress based FLD criterion. The optimization software HEEDS (Hierarchical Evolutionary Engineering Design System) was used in combination with the nonlinear structural finite element code LS-DYNA to carry out the numerical investigation.

The optimal temperature values for the different sections, i.e. punch, blank, upper- and lower-die, were to be determined so as to maximize the punch displacement while satisfying the forming limit diagram (FLD). The FLD provides information about how much a particular structure can be deformed before necking occurs. Principal strains for each element of the blank must lie below the major strain vs. minor strain curve of the forming limit diagram to avoid bursting (or stresses for the σ-FLD). In this analysis, a temperature-dependent FLD was used. By first curve fitting each FLD at a particular temperature, the coefficients of the different FLD curves were then fit with appropriate functions to create a master FLD for all temperatures. The temperature dependent FLD was then incorporated into the UMAT in order to check each element for failure.

The characteristics of the design space associated with the current optimization problem were not known *a priori*. In this case, it was advisable to employ a combination of global and local search techniques in order to achieve a broad and effective search for an optimal solution. For such problems, HEEDS utilizes a combination of evolutionary, gradient based, and design of experiments search heuristics.

HEEDS applies several optimization methods simultaneously, allowing each method to take advantage of the best attributes and solutions found from other parallel searches. The multiple semi-independent search processes exchange information about the solution space with each other, helping to jointly satisfy multiple constraints and objectives. This

search method is called a *heterogeneous multi-agent approach*. This approach quickly identifies design attributes with good potential and uses them to focus, improve and accelerate the search for an optimum solution. More details about the HEEDS program could be found at www.redcedartech.com.

For the warm forming analysis of the hemispherical punch, the variables for the optimization process were the temperatures for the punch, blank, upper- and lower-die. The variables were allowed to vary between specified minimum and maximum values. The punch and blank temperatures were allowed to change without any pre-specified conditions. The temperature of the upper- and lower-die, however, were linked to the blank temperature because of the current experimental setup (Abedrabbo et al., 2006b) where the band heaters were placed on the outside of the die and the blank was heated accordingly. A separate temperature variable for each part could be used in the optimization process, depending on the design of the experimental setup for a specific part. Therefore, in the current setup, the upper- and lower-die were assigned to vary as much as 10 °C higher than the blank.

After running the optimization problem for the current experiment, the HEEDS program was able to reach an "optimum" solution after about 25 iterations for the AA5754-O material. The maximum punch displacement found for the AA5754-O material was 37.45 mm (1.48 in.), corresponding to iteration number 30. Fig. 22 shows the punch displacement vs. number of HEEDS evaluations, while Fig. 23 shows the temperatures of the punch and the blank vs. number of HEEDS evolutions. As can be seen, any temperature set corresponding to a HEEDS' evaluation higher than 25 would give a

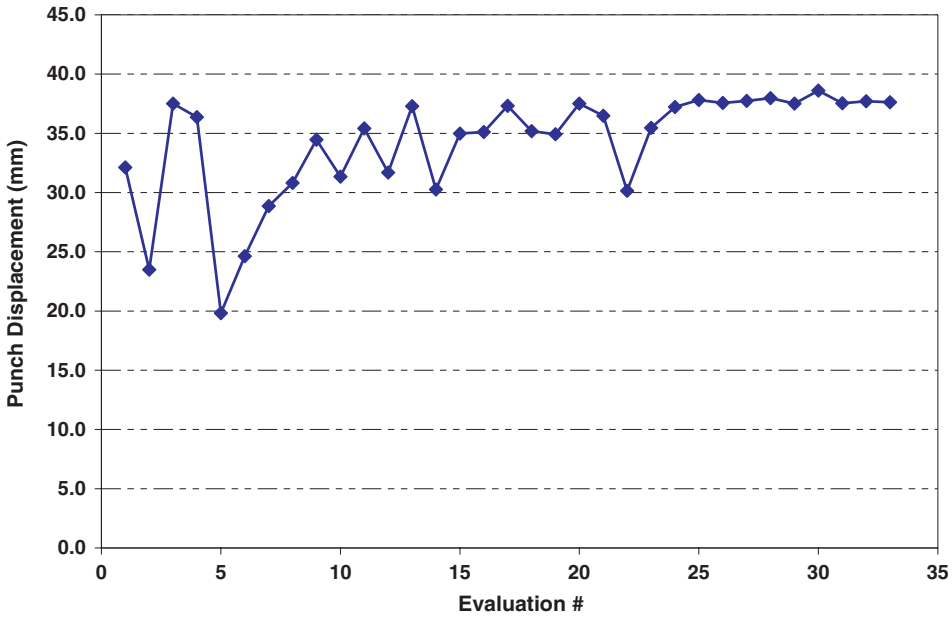

Fig. 22. HEEDS optimization process result showing punch displacement vs. number of HEEDS evaluations for AA5754-O. An "optimum" solution is reached after ~25 evaluations. Maximum punch displacement is found at evaluation no. 30.

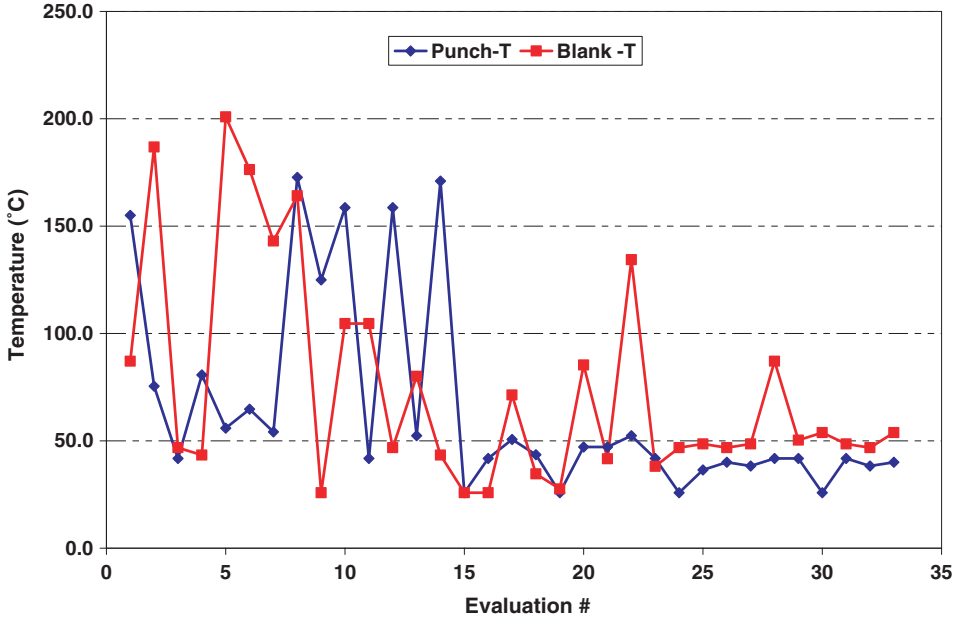

Fig. 23. HEEDS optimization process result showing punch and blank temperatures vs. number of HEEDS evaluations for AA5754-O. An "optimum" solution is reached after ~25 evaluations. Optimum solution is found at evaluation no. 30. Upper and lower-die temperatures are set to 10 °C higher than blank temperature.

satisfactory solution to the problem of maximizing formability for the current setup. Punch displacement, temperatures of different components, and the corresponding evaluation number are given in Table 9, with the maximum set for formability in bold.

An interesting fact that Table 9 reveals is that a higher temperature is not needed to form the part; instead the punch should be maintained at the lowest temperature possible for maximum formability. A comparison of the maximum punch displacement for the optimum case (63.85 °C) and that in Fig. 21 (177 °C) shows that an extra 0.1 in. punch travel can be achieved prior to failure using a lower die temperature, as long as the punch temperature could be maintained at (25.85 °C). This was expected since, as explained by Abedrabbo et al. (2006b), the greater forming depths achieved at elevated temperatures were attributed to the temperature gradient between the blank and the punch. When

Table 9
HEEDS results for the AA5754-O material showing values of punch displacement and temperatures of the punch, blank and dies corresponding to the "best" evaluations

Evaluation no.	Punch displacement (mm)	Punch temperature (°C)	Blank temperature (°C)	Upper and lower die temperature (°C)
26	36.56	40.01	46.85	56.85
27	36.74	38.24	48.60	58.60
28	36.96	41.78	87.10	97.10
29	36.50	41.78	50.35	60.35
30	**37.45**	**25.85**	**53.85**	**63.85**

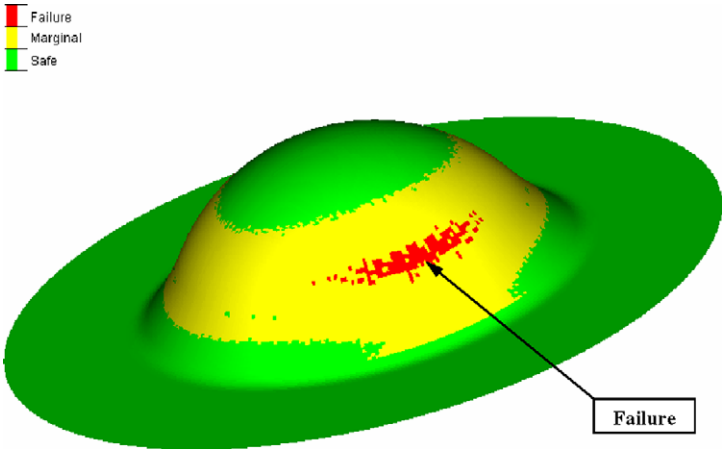

Fig. 24. Finite element result from a fully coupled thermo-mechanical simulation of thermo-forming for AA5754-O using temperatures for different parts corresponding to HEEDS evaluation no. 30 (Table 9). Graph shows contour plots of formability using stress based FLD where minor- and major-true stresses for each element are projected on the sheet. Failure location is shown. The sheet failed where the stresses crossed the σ-FLD curve (as shown in Fig. 25) at the punch depth of 37.5 mm (1.48 in.).

the punch is kept at a lower temperature than the blank, those areas of the blank that come into contact with the punch would lose heat and therefore become at a lower temperature level (become stronger) than the unsupported areas of the blank. As the punch

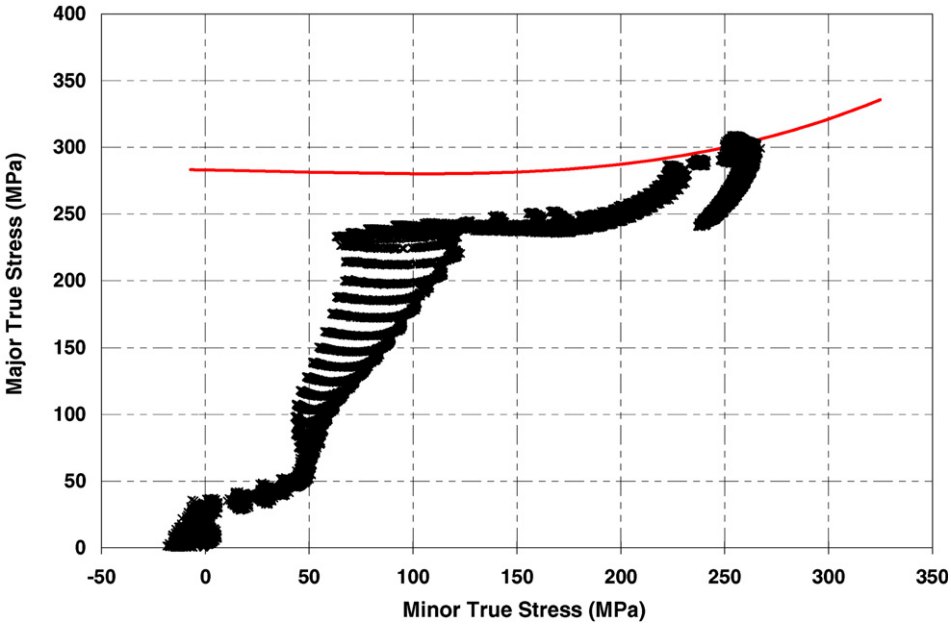

Fig. 25. Plot of major true stress vs. minor true stress for the fully coupled thermo-mechanical simulation of AA5754-O as shown in Fig. 24. Graph shows contour plots of formability using stress based FLD. The sheet failed where the stresses crossed the σ-FLD curve (line) at the punch depth of 37.5 mm (1.48 in.).

traveled, the unsupported regions of the blank (regions not in contact with the punch) would stretch more due to their lower tensile strength.

Fig. 24 shows the fully coupled thermo-mechanical simulation result of pure stretching of AA5754-O using the "optimal" set of temperatures for different parts found by HEEDS at evaluation no. 30 from Table 9 with failure location indicated. The figure shows the contour of minor-true stress and major-true stress on each element. The failure prediction area shown is based on the stress based FLD (σ-FLD). Fig. 25 shows a plot of the major true stress vs. minor true stress for every element in the sheet. Failure occurred for those elements that crossed the stress based limit curve (σ-FLD).

The optimization process introduced here is currently being used to study the viability of the warm forming process to form complex automotive parts, e.g. door panel, license plate pocket, etc. using aluminum alloys.

11. Conclusions

A temperature-dependent anisotropic material model for finite element analysis and formability simulation has been developed for two automotive aluminum alloys, AA5182-O and AA5754-O. Through the use of experimental data from multiple uniaxial tests in different directions, the anisotropy coefficients of the Barlat YLD2000-2d model for several elevated temperatures in the range of 25–260 °C (77–500 °F) have been calculated. The anisotropy coefficients of the yield function were determined as a function of temperature using appropriate polynomial curve fit functions. A strain-rate dependent hardening flow rule was also determined as a function of temperature using experimental results.

The developed temperature-dependent anisotropic material model was then successfully implemented as a user material subroutine (UMAT) in the finite element code LS-DYNA to be used in a fully coupled thermo-mechanical finite element analysis of the warm forming of aluminum products.

Forming limit diagrams were developed for the two materials by two methods: strain based FLD's (ε-FLD) from the M–K method; and the stress-based FLD (σ-FLD). Both models were developed using Barlat's anisotropic yield function YLD2000-2d.

Finite element analysis with the developed thermo-mechanical constitutive model accurately predicted both the deformation behavior and the failure location in the blank and compared favorably to the experimental results for both materials. The current research shows the importance of using both thermal analysis and an accurate anisotropic temperature-dependent material model in a fully coupled mode in order to model the warm forming process accurately. Although the current thermoforming analysis was only verified for biaxial stretching, its application to more complex parts is also expected to yield accurate results. This is because the accuracy of the YLD2000-2d (and YLD96) yield function at room temperature has already been thoroughly verified by many researchers. Therefore, to expect similar performance at elevated temperature is not unreasonable.

An optimization program was used to find the "optimum" set of temperatures for the different components that would give the maximum formability for the pure stretch of a hemispherical punch. The program was capable of finding multiple temperatures that could be used to form the current part. This process will be used to simulate the formability of more complex automotive parts, where the temperatures of the different sections will be determined automatically.

Acknowledgements

The authors thank General Motors for their support of this research project, and Red Cedar Technology for their assistance in running the optimization program HEEDS. The authors especially thank Drs. Paul Krajewski, Anil Sachdev, Jim Schroth and Tom Stoughton from the GM Research and Development Center and Dr. Frederic Barlat from ALCOA for their assistance and helpful discussions in support of this research.

References

Abedrabbo, N., Pourboghrat, F., Carsley, J., 2006a. Forming of aluminum alloys at elevated temperatures – Part 1: Material characterization. Int. J. Plasticity 22 (2), 314–341.

Abedrabbo, N., Pourboghrat, F., Carsley, J., 2006b. Forming of aluminum alloys at elevated temperatures – Part 2: Numerical modeling and experimental verification. Int. J. Plasticity 22 (2), 342–737.

Abedrabbo, N., 2005. Forming of aluminum alloys at elevated temperatures. Ph.D. Dissertation, Michigan State University.

Abedrabbo, N., Zampaloni, M., Pourboghrat, F., 2005. Wrinkling control in aluminum sheets using stamp hydroforming. Int. J. Mech. Sci. 47 (3), 333–358.

Armero, F., Simo, J.C., 1993. A priori stability estimates and unconditionally stable product formula algorithms for nonlinear coupled thermoplasticity. Int. J. Plasticity 9 (6), 749–782.

Auricchio, F., Taylor, R.L., 1999. A return-map algorithm for general associative isotropic elasto-plastic materials in large deformation regimes. Int. J. Plasticity 15 (12), 1359–1378.

Ayres, R.A., 1979a. Alloying aluminum with magnesium for ductility at warm temperatures (25 to 250 °C). Met. Trans. A 10, 849–854.

Ayres, R.A., Wenner, M.L., 1979b. Strain and strain-rate hardening effects in punch stretching of 5182-O aluminum at elevated temperatures. Met. Trans. A 10, 41–46.

Barlat, F., Aretz, H., Yoon, J.W., Karabin, M.E., Brem, J.C., Dick, R.E., 2005. Linear transformation-based anisotropic yield functions. Int. J. Plasticity 21 (5), 1009–1039.

Barlat, F., Brem, J.C., Yoon, J.W., Chung, K., Dick, R.E., Lege, D.J., Pourboghrat, F., Choi, S.H., Chu, E., 2003. Plane stress yield function for aluminum alloy sheets – Part 1: Theory. Int. J. Plasticity 19, 1297–1319.

Barlat, F., Richmond, O., 2003. Modelling macroscopic imperfections for the prediction of flow localization and fracture. Fatigue Fract. Eng. Mater. Struct. 26 (4), 311–321.

Barlat, F., Maeda, Y., Chung, K., Yanagawa, M., Brem, J.C., Hayashida, Y., Lege, D.J., Matsui, K., Murtha, S.J., Hattori, S., Becker, R.C., Makosey, S., 1997. Yield function development for aluminum alloy sheets. J. Mech. Phys. Solids 45 (11/12), 1727–1763.

Barlat, F., Lege, D.J., Brem, J.C., 1991. A six-component yield function for anisotropic metals. Int. J. Plasticity 7, 693–712.

Boogaard, A.H. van den, Bolt, P.J., Werkhoven, R.J., 2001. Aluminum sheet forming at elevated temperatures. In: Mori, K.-I. (Ed.), Simulation of Materials Processing: Theory, Methods and Applications. A.A. Balkema, Lisse, pp. 819–824.

Čanađija, M., Brnić, J., 2004. Associative coupled thermoplasticity at finite strain with temperature-dependent material parameters. Int. J. Plasticity 20 (10), 1851–1874.

Chung, K., Wagoner, R.H., 1998. Invariance of plastic strains with respect to imposed rate at boundary. Met. Mater. 4 (1), 25–32.

Chung, K., Lee, S.Y., Barlat, F., Keum, Y.T., Park, J.M., 1996. Finite element simulation of sheet forming based on a planar anisotropic strain-rate potential. Int. J. Plasticity 12 (1), 93–115.

Chung, K., Richmond, O., 1993. A deformation theory of plasticity based on minimum work paths. Int. J. Plasticity 9 (8), 907–920.

Chung, K., Shah, K., 1992. Finite element simulation of sheet metal forming for planar anisotropic metals. Int. J. Plasticity 8 (4), 453–476.

Chung, K., Wagoner, R.H., 1986. Invariance of necking formation to material strength and strain rate for power-law materials. Metall. Trans. 17A, 1632–1633.

Green, D.E., Neale, K.W., MacEwen, S.R., Makinde, A., Perrin, R., 2004. Experimental investigation of the biaxial behaviour of an aluminum sheet. Int. J. Plasticity 20 (8–9), 1677–1706.

Greene, D.L., DiCicco, J., 2000. Engineering-economic analyses of automotive fuel economy potential in the United States. ORNL/TM-2000/26, Oak Ridge National Laboratory, Oak Ridge, TN.

Gronostajski, Z., 2000. The constitutive equations for FEM analysis. J. Mater. Proc. Tech. 106, 40–44.

Håkansson, P., Wallin, M., Ristinmaa, M., 2005. Comparison of isotropic hardening and kinematic hardening in thermoplasticity. Int. J. Plasticity 21 (7), 1435–1460.

Hallquist, J.O., 1999. LS-DYNA User's manual. Livermore Software Technology Corporation, CA.

Hashiguchi, K., 2005. Generalized plastic flow rule. Int. J. Plasticity 21 (2), 321–351.

Han, C.S., Chung, K., Wagoner, R.H., Oh, S.I., 2003. A multiplicative finite elasto-plastic formulation with anisotropic yield functions. Int. J. Plasticity 19 (2), 197–211.

HEEDS (Hierarchical Evolutionary Engineering Design System) Getting Started Manual, Red Cedar Technology, MI, 48823, USA. Available from: <www.redcedartech.com>.

Hill, R., 1948. A theory of the yielding and plastic flow of anisotropic metals. Proc. Roy. Soc. Lond. Ser. A 193, 281–297.

Kim, K.J., Kim, D., Choi, S.H., Chung, K., Shin, K.S., Barlat, F., Oh, K.H., Youn, J.R., 2003. Formability of AA5182/polypropylene/AA5182 sandwich sheets. J. Mater. Proc. Tech. 139 (1–3), 1–7.

Lademo, O.G., 1999a. Engineering models of elastoplasticity and fracture for aluminum alloys. PhD. Thesis, Norvegian Institute of Science and Technology, Trondheim, Norway, 1999.

Lademo, O.G., Hopperstad, O.S., Langseth, M., 1999b. An evaluation of yield criteria and flow rules for aluminum alloys. Int. J. Plasticity 15, 191–208.

Li, D., Ghosh, A., 2004. Biaxial warm forming behavior of aluminum sheet alloys. J. Mater. Proc. Tech. 145, 281–293.

Li, D., Ghosh, A., 2003. Tensile deformation behavior of aluminum alloys at warm forming temperatures. Mater. Sci. Eng. A 352, 279–286.

Marciniak, Z., Kuczynski, K., 1967. Limit strains in the processes of stretch-forming sheet metal. Int. J. Mech. Sci 9 (9), 609–612.

Naka, T., Torikai, G., Hino, G., Yoshida, F., 2001. The effects of temperature and forming speed on the forming limit diagram for type 5083 aluminum-magnesium alloy sheet. J. Mater. Proc. Tech. 113, 648–653.

Painter, M.J., Pearce, R., 1980. The elevated temperature behavior of some Al–Mg alloys. Les Mâemoires Scientifiques De La Revue Mâetallurgie 77, 617–634.

Robinson, J.M., Shaw, M.P., 1994. Microstructural and mechanical influences on dynamic strain aging phenomena. Int. Mater. Rev. 39, 113–122.

Schroth, J.G., 2004. General Motors' quick plastic forming process. In: Taleff, E., Friedman, P.A., Krajewski, P.E., Mishra, R.S., Schroth, J.G. (Eds.), Advances in Superplasticity and Superplastic Forming. TMS, Warrendale, PA, pp. 9–20.

Simo, J.C., Hughes, T.J.R., 1998. Computational Inelasticity. Springer, New York, pp. 143–149.

Stoughton, T.B., 2001. Stress-based forming limits in sheet metal forming. J. Eng. Mater. Tech. 123, 417–422.

Stoughton, T., Zhu, X., 2004. Review of theoretical models of the strain-based FLD and their relevance to the stress-based FLD. Int. J. Plasticity 20 (8–9), 1463–1486.

Takata, K., Ohwue, T., Saga, M., Kikuchi, M., 2000. Formability of Al–Mg alloy at warm temperature. Mater. Sci. Forum (331–337), 631–636.

Tuğcu, P., Neale, K.W., 1999. On the implementation of anisotropic yield functions into finite strain problems of sheet metal forming. Int. J. Plasticity 15 (10), 1021–1040.

Vegter, H., Boogaard, A.H. van den, 2006. A plane stress yield function for anisotropic sheet material by interpolation of biaxial stress states. Int. J. Plasticity 22 (3), 557–580.

Voyiadjis, G.Z., Abed, F.H., 2006. A coupled temperature and strain rate dependent yield function for dynamic deformations of bcc metals. Int. J. Plasticity 22 (8), 1398–1431.

Wagoner, R.H., Chenot, J.-L., 1996. In: Fundamentals of Metal Forming. Wiley, New York, pp. 10–31.

Wagoner, R.H., Nakamachi, E., Germain, Y., 1988. Analysis of sheet forming operations using the finite element method. In: Proceedings of IDDRG Working Groups, Toronto, p. 1.

Wriggers, P., Miehe, C., Kleiber, M., Simo, J.C., 1992. On the coupled thermomechanical treatment of necking problems via finite-element methods. Int. J. Numer. Meth. Eng. 33 (4), 869–883.

Wu, P.D., MacEwen, S.R., Lloyd, D.J., Jain, M., Tugcu, P., Neale, K.W., 2005. On pre-straining and the evolution of material anisotropy in sheet metals. Int. J. Plasticity 21 (4), 723–739.

Yao, H., Cao, J., 2002. Prediction of forming limit curves using an anisotropic yield function with prestrain induced backstress. Int. J. Plasticity 18, 1013–1038.

Yoon, J.W., Barlat, F., Dick, R.E., Karabin, M.E., 2006. Prediction of six or eight ears in a drawn cup based on a new anisotropic yield function. Int. J. Plasticity 22 (1), 174–193.

Yoon, J.W., Barlat, F., Dick, R., Chung, K., Kang, T.J., 2004. Plane stress yield function for aluminum alloy sheets – Part II: FE formulation and its implementation. Int. J. Plasticity 20 (3), 495–522.

Yoon, J.W., Yang, D.Y., Chung, K., Barlat, F., 1999. A general elasto-plastic finite element formulation based on incremental deformation theory for planar anisotropy and its application to sheet metal forming. Int. J. Plasticity 15 (1), 35–67.

Zampaloni, M., Abedrabbo, N., Pourboghrat, F., 2003. Experimental and numerical study of stamp hydroforming of sheet metals. Int. J. Mech. Sci. 45 (11), 1815–1848.